POLITECNICO
MILANO 1863

SCUOLA DI INGEGNERIA INDUSTRIALE
E DELL'INFORMAZIONE

A FRACTURE MECHANICS APPROACH TO THE ENVIRONMENTAL STRESS CRACKING OF HIPS

MATERIALS ENGINEERING AND
NANOTECHNOLOGY MASTER THESIS

Author: Lorenzo Tamaro

Student ID:	10742541
Advisor:	Luca Andena
Co-advisor:	Marco Contino
Academic Year:	2021-22

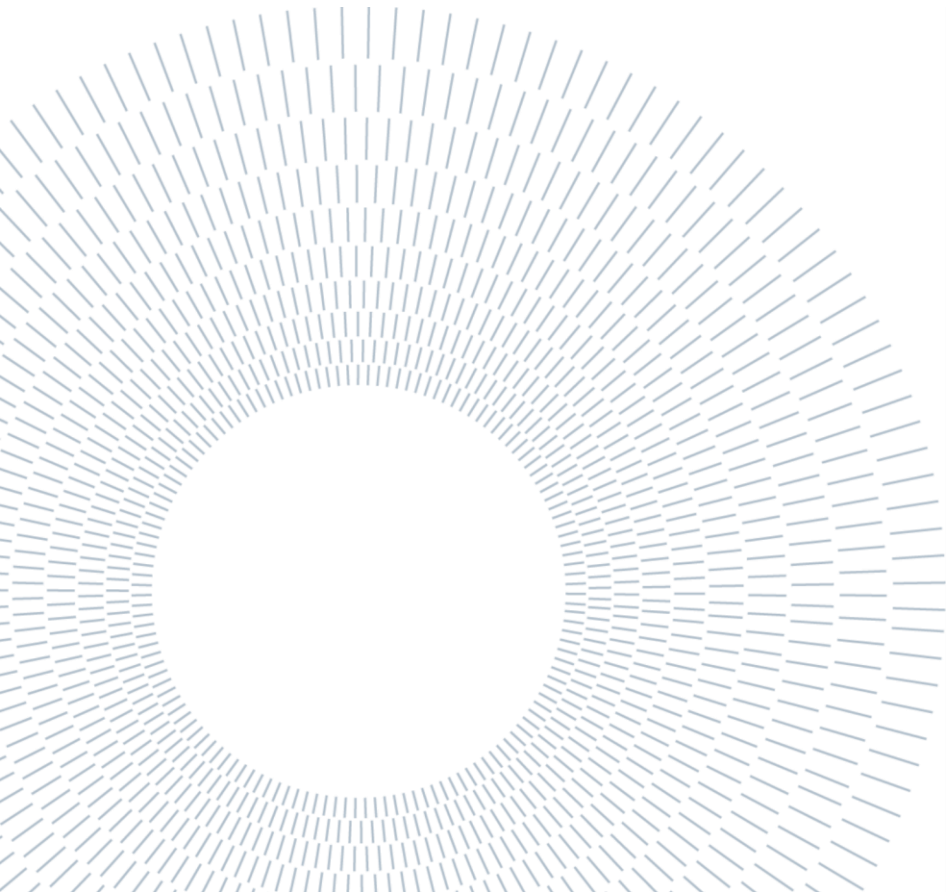

Abstract

Keywords: polymers, linear elastic fracture mechanics, environmental stress cracking, HIPS, time-temperature equivalence, lifetime prediction

In this work the Environmental Stress Cracking (ESC) resistance of two high-impact polystyrene (HIPS) grades, a general purpose one and an ESC-resistant one, was evaluated following a Linear-Elastic Fracture Mechanics approach by developing a script to automate the process of data elaboration. The active environment of choice was sunflower oil, which is known to interact with these materials.

Tests in the four-point bending configuration were performed on notched samples at constant load (creep) and constant displacement rate. From these tests, the fracture behavior of the materials was characterized by analyzing both the crack initiation and propagation phase, for tests both in air and in active environment. The characterization was done using both stress intensity factor, K and energy release rate, G, as relevant fracture parameters.

The analysis of this data is a long process that passes through many intermediate steps. In this work the possibility of using an automated method to speed up this process.

Specifically, 2 scripts have been written, one for each testing configuration. These permits, where possible, to make automatic the analysis starting directly from raw data coming from testing instruments.

Some considerations are then made on the possibility to use these scripts instead of analyzing the specimen data one by one.

Abstract in lingua italiana

Parole chiave: polimeri, meccanica della frattura lineare elastica, environmental stress cracking, HIPS, equivalenza tempo-temperatura, previsione tempo di vita.

In questo lavoro, la resistenza ad *Environmental Stress Cracking* di due gradi di polistirene antiurto (HIPS), uno per applicazioni generiche e uno specifico per contatto con ambiente attivo, è stata valutata usando un approccio basato sulla meccanica della frattura lineare elastica scrivendo degli script in grado di rendere automatica l'elaborazione dei dati. L'ambiente attivo utilizzato è l'olio di semi di girasole, essendone nota l'interazione con i materiali utilizzati.

Test di frattura in flessione a quattro punti sono stati condotti su provini intagliati sotto carico costante (*creep*) e con velocità di deformazione costante. Da questi test il comportamento a frattura dei materiali usati è stato caratterizzato analizzando sia la fase di innesco della frattura che la seguente fase di propagazione, in aria come in ambiente attivo. Questa caratterizzazione è stata fatta utilizzando sia il fattore di intensificazione degli sforzi, K, che il tasso di rilascio di energia, G, come parametri di frattura.

L'analisi di questi dati è un processo che richiede di passare attraverso diversi passaggi di elaborazione intermedi. In questo lavoro, viene esplorata la possibilità di utilizzare un metodo automatico per rendere più veloce questo processo.

Nello specifico, sono stati elaborati 2 script da utilizzare ciascuno per una configurazione di test (creep o a velocità di deformazione costante). Questi script permettono, per quanto possibile, di rendere automatica l'analisi partendo direttamente dai dati raw estratti dagli strumenti di test.

Vengono poi fatte delle considerazioni sull'effettiva possibilità di utilizzare soltanto questo metodo automatizzato di analisi al posto dell'analisi manuale dato per dato.

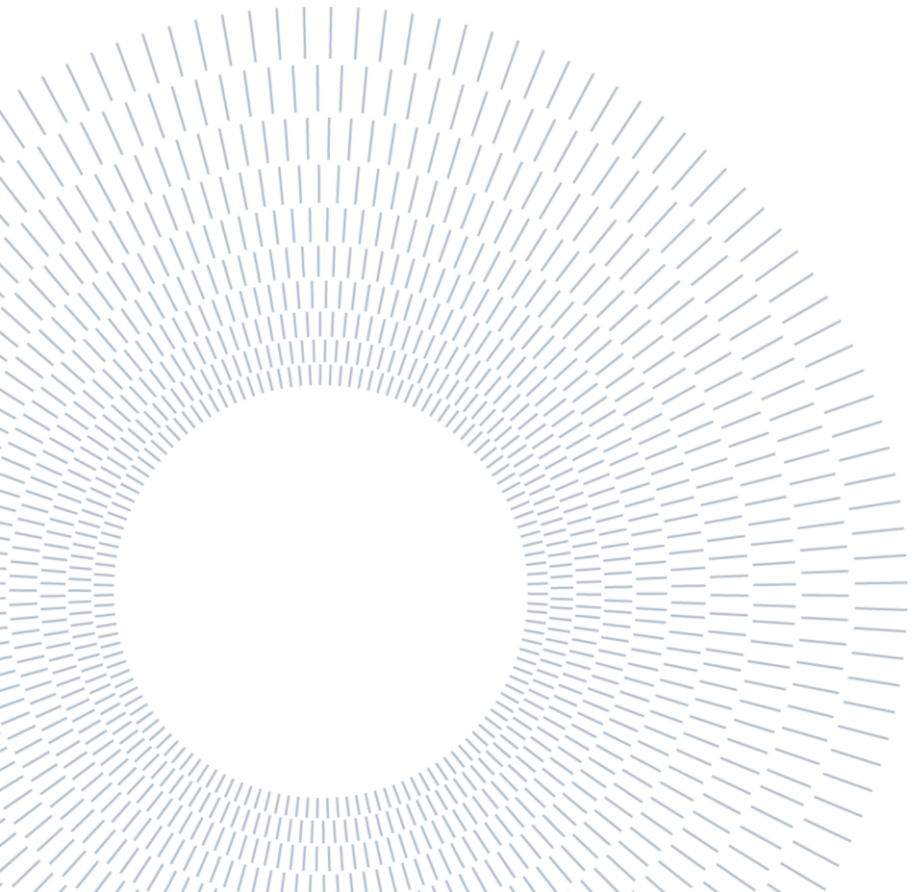

Contents

Introduction

HIPS is widely used in many everyday applications, one of them being as the interior material for the building of fridges. In such an application, it can easily come in contact with an oil of some type. This can be dangerous for the life of the component because of a particular interaction mechanism between the material and the oil. This is known as Environmental Stress Cracking (ESC), which can lead to the premature failure of the component. The aim of the study is to investigate ESC on HIPS with a fracture mechanics based approach, with a focus on being able to predict the long-term fracture behavior of this material. This project was also conducted as a part of a bigger project involving many other laboratories involved in the ESIS TC4 (European structural integrity society technical committee 4), where the reproducibility of the measurements done in this work will be verified.

This work is organized in 5 chapters, with the following structure: Chapter 1 gives the theoretical background, reporting on the main theories used in this work and on the state of the art for the study of environmental stress cracking. Chapter 2 describes the materials analyzed in this work and specimen preparation. Chapter 3 explains the experimental techniques used. Chapter 4 finally reports and comments on the two scripts developed to automate the analysis of the obtained raw data. Chapter 5 presents some conclusions which can be taken from this work.

1 Theoretical background

1.1 High Impact Polystyrene

High Impact Polystyrene is a polymer which is derived from polystyrene. Polystyrene is a thermoplastic polymer which is usually produced by radical polymerization of styrene. It is widely employed in the food-service industry in products such as rigid

trays, containers and disposable utensils. It has many advantageous properties but has one main drawback: it is brittle. To improve this property, styrene can be polymerized in the presence of some rubber particles. It is known that dispersing rubber particles inside a polymer is a great way to increase its tenacity [1]. When doing so, the final product takes the name of High Impact Polystyrene (HIPS). HIPS grades contain usually between 6% and 10% of polybutadiene in the form of spheres with diameters ranging from 0.5 to 5 μm, the specific distribution of these spheres influences the properties of the final material. Actually, as can be seen in Figure 1, polybutadiene spheres do not present a homogeneous structure. Instead, only 20% of the total volume of the sphere is composed by the continuum of the rubber phase, and the remaining 80% is the styrenic matrix.

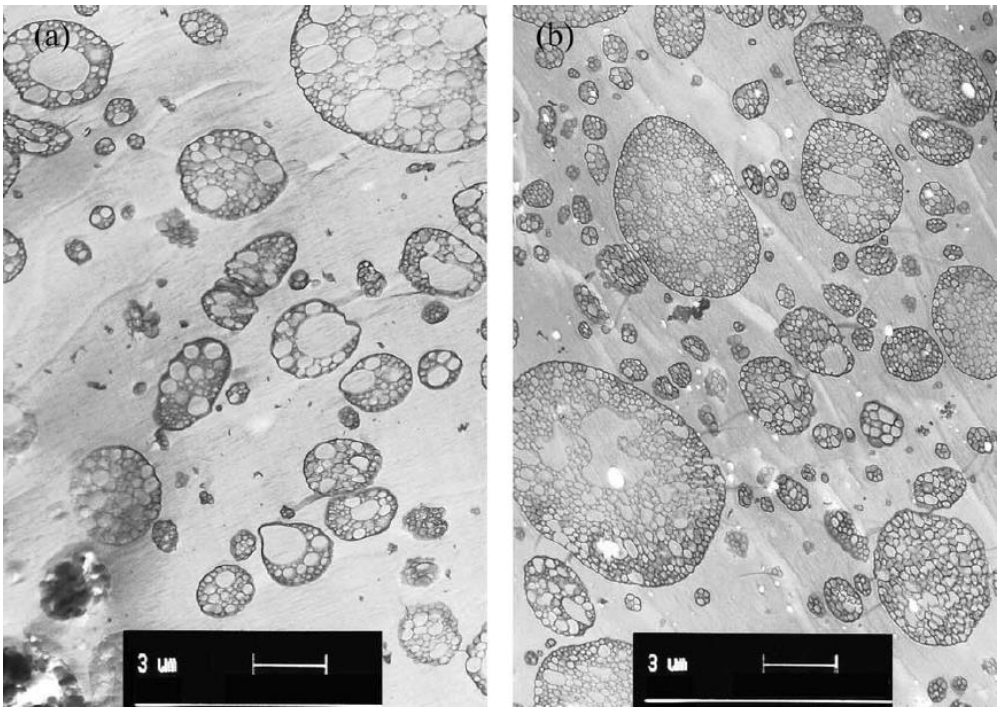

Figure 1: TEM micrographs of HIPS samples (Grassi2011)

The reason behind this increase in toughness is to be attributed to the energy absorbed by the crazing yielding mechanism, which will be examined later in this chapter. In normal conditions polystyrene presents a brittle behavior, but the addition of polybutadiene favors highly localized plastic deformations. Upon macroscopically deforming the material, rubber particles are able to generate in their surroundings lots of microcrazes, which contribute to absorbing a high amount of energy. Thanks to the increase in toughness given by the addition of the rubber phase, HIPS is widely used

in many fields, one of them being the food packaging and in stores displays, as it is also a good printable substrate.

HIPS was the material tested in this work, and its mechanical resistance has been tested. When a high enough load is applied on a HIPS artifact, in general it gets damaged following some steps, which are deformation, yielding and fracture. All of these steps have been examined in the following sections. To understand the deformation of polymers, it is important to introduce the concept of viscoelasticity.

1.2 Viscoelasticity

Viscoelasticity is the property of materials that exhibit a combination of elastic and viscous behavior when undergoing deformation. When a material exhibiting perfectly elastic properties is loaded, stress is always directly proportional to strain in small deformations, and it is independent from the rate of strain. On the other hand, a perfectly viscous material (a fluid in this case) obeys Newton's law, for which the stress is directly proportional to the rate of strain and independent on the value of the strain. These are of course idealizations. So, a viscoelastic material presents a combination of these 2 responses. All polymers present viscoelastic properties due to their internal structure characterized by long polymeric chains. An important aspect of viscoelastic materials deriving from these considerations is that the deformation output is time (and history) dependent.

The nature of polymers can be described by suitable viscoelastic functions. The two most common ones are the creep compliance and the relaxation modulus. They can be

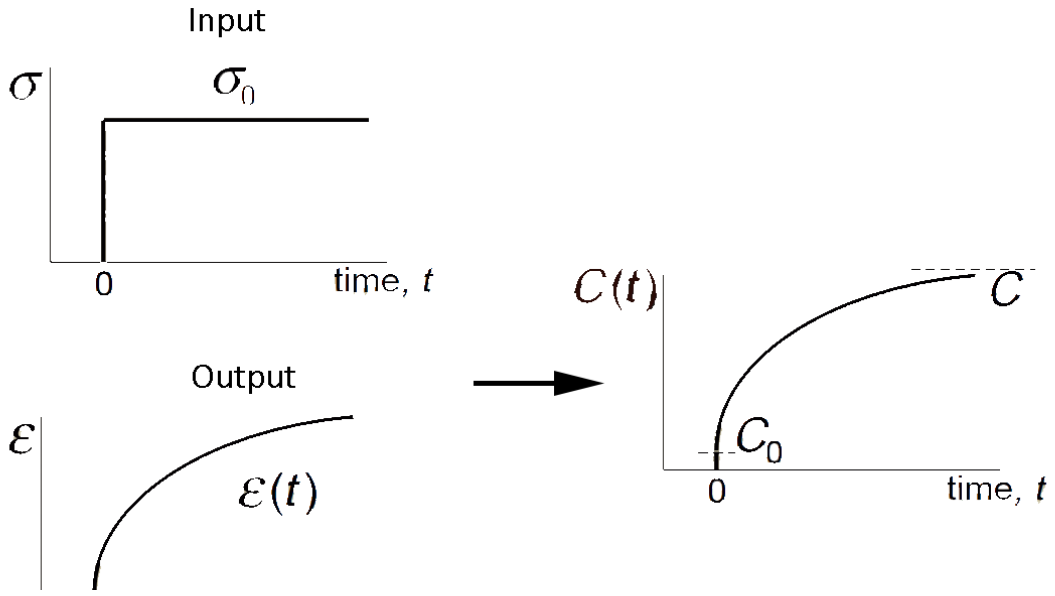

Figure 2: Scheme of a creep experiment

determined conducting relevant tests: creep and relaxation, respectively. A creep test ideally consists in the instantaneous application of a load which is then maintained constant for the whole duration of the test, as schematized in Figure 2.

The relaxation test consists, instead, in the instantaneous application of a deformation which is then kept constant. The obtained outputs of these tests are respectively a deformation and a stress. From these, the viscoelastic functions are computed as the ratio between the output and the input.

Another concept to introduce in this discussion is the one of linearity. If a material is linearly viscoelastic, the output is proportional to the input (considered at the same time). This is important since in this regime the compliance and the modulus will be a material property independent on the magnitude of the applied input.

In materials exhibiting linearity, the Boltzmann's superposition postulate can be applied. The idea behind it is that the effects of different inputs are independent from each other, and so the output of a test can be analyzed as the sum of the output of each individual input. A schematization of this concept is shown in Figure 3.

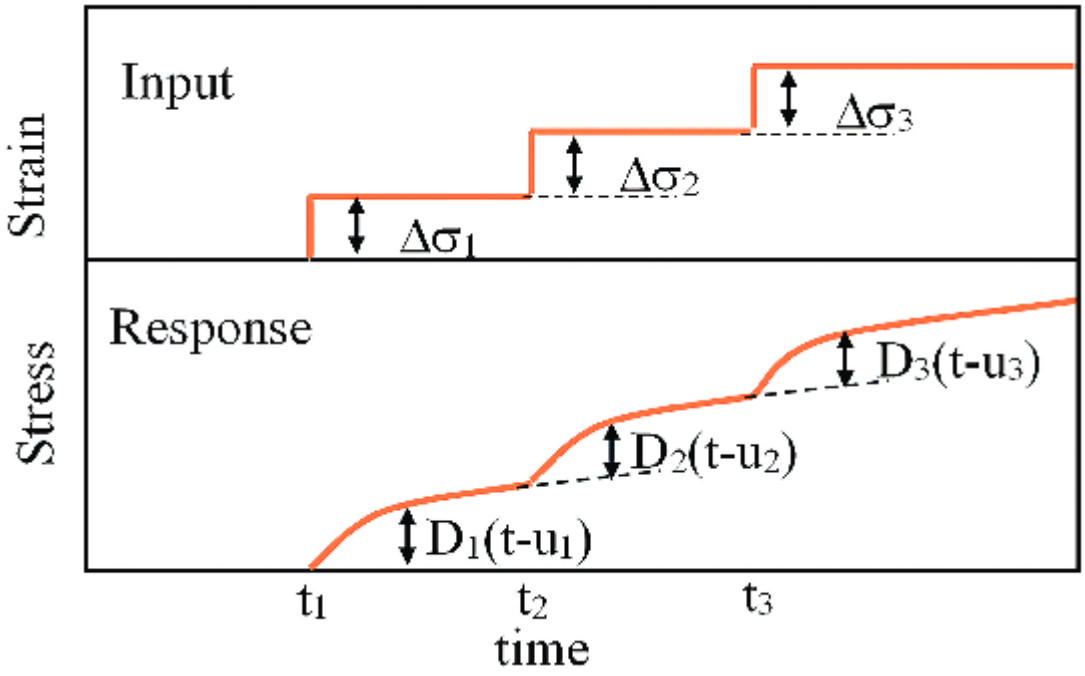

Figure 3: scheme of the Boltzmann's superposition postulate [2]

This can be applied also if the variations in the inputs are continuous and not discrete. In this case the problem can be solved by means of the Boltzmann's integrals:

$$\epsilon(t) = \int_{t'=0}^{t'=t} D(t-t')\frac{d\sigma(t')}{dt'}dt' \qquad (1\text{-}1)$$

$$\sigma(t) = \int_{t'=0}^{t'=t} E(t-t')\frac{d\epsilon(t')}{dt'}dt' \tag{1-2}$$

Here, D and E are called memory functions and by means of these integrals it is possible to determine the material's response to any stress or strain history applied, provided the memory functions are known.

Viscoelastic functions are known to be dependent also on temperature since this factor accelerates the kinetics of the deformation process. If the material under analysis is thermorheologically simple, this dependence can be described via the time-temperature superposition postulate.

1.3 Time-temperature superposition

Polymers are known to present a direct correlation between time and temperature. In particular, being them viscoelastic materials, temperature greatly affects their viscoelastic response. In most polymers, the temperature has an influence only on the kinetic of the processes leaving unaffected its nature, at least in some temperature ranges. These polymers are known as thermo-rheologically simple and for them the time-temperature superposition postulate applies [3]: when a mechanical property (such as the relaxation modulus or the creep compliance) is measured at different temperature and represented on a logarithmic time-scale, the shape of the curve remains the same and it is simply translated along the time axis as the temperature is varied. The amount of shift needed to superimpose two curves is known as the shift factor between the two considered temperatures. This can be extremely useful from the experimental point of view since it can allow us to perform some experiments that would require a long time in a much shorter one by just performing them at a higher temperature, speeding up the process.

The shift factor is a property of the material and is defined with respect to an arbitrary reference temperature. There are two relations that are used to express the dependence of the shift factor on temperature, and their applicability depends on the temperature in relation to the T_g of the material. For temperatures below T_g an Arrhenius-type relation is usually considered, in particular:

$$\log\left(a_T^{T_0}\right) = \frac{\Delta H}{R}\left(\frac{1}{T} - \frac{1}{T_0}\right) \tag{1-3}$$

where ΔH is an activation energy and R is the gas constant. Above T_g, the Williams-Landel-Ferry equation is used instead:

$$\log\left(a_T^{T_0}\right) = -\frac{C_1(T - T_0)}{C_2 + (T - T_0)} \tag{1-4}$$

where C_1 and C_2 are material's constants. From these relations it is possible to build a so-called master curve at the reference temperature. In this master curve, the property under investigation is represented on a very broad time interval, much broader than actual time window of the experiments.

These considerations obviously apply to viscoelastic functions such as the creep compliance and the relaxation modulus. An example on how a master curve is built is reported in Figure 4.

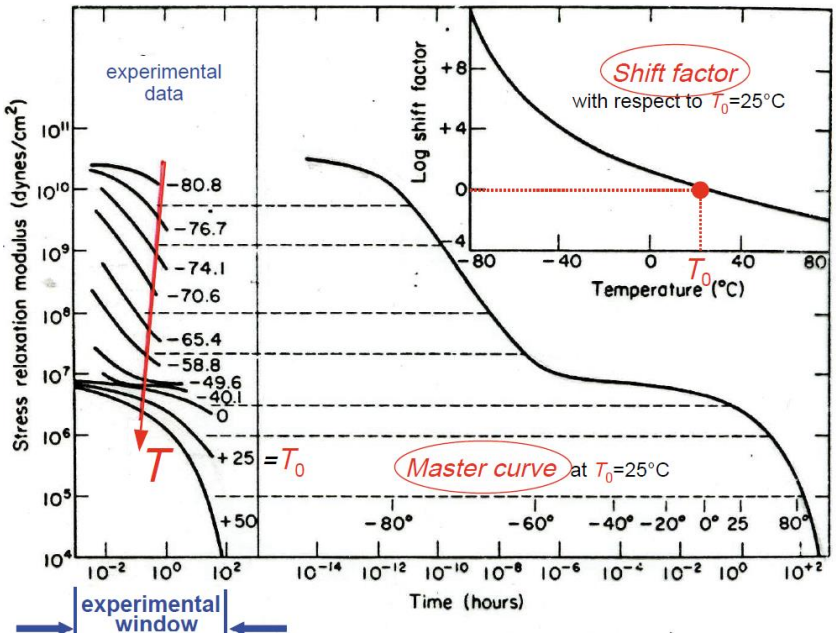

Figure 4: Building of a master curve for the stress relaxation of polyisobutylene [3]

When a certain value of deformation is exceeded, deformations become no longer (visco)elastic, but (visco)plastic, meaning that the material is getting permanently damaged. There are different mechanisms with which this can happen, and they will be treated in the next section.

1.4 Yielding mechanisms

There are mainly two mechanisms of yielding in polymers, which are shear yielding and crazing. Shear yielding is a distortional plasticity occurring at constant volume. The distortion occurs within a narrow band (named shear band), where fibrils get

stretched. These bands are widely diffused in the volume, there are many of them and they cross each other [4]. Crazing is a form of dilatational plasticity; it causes the

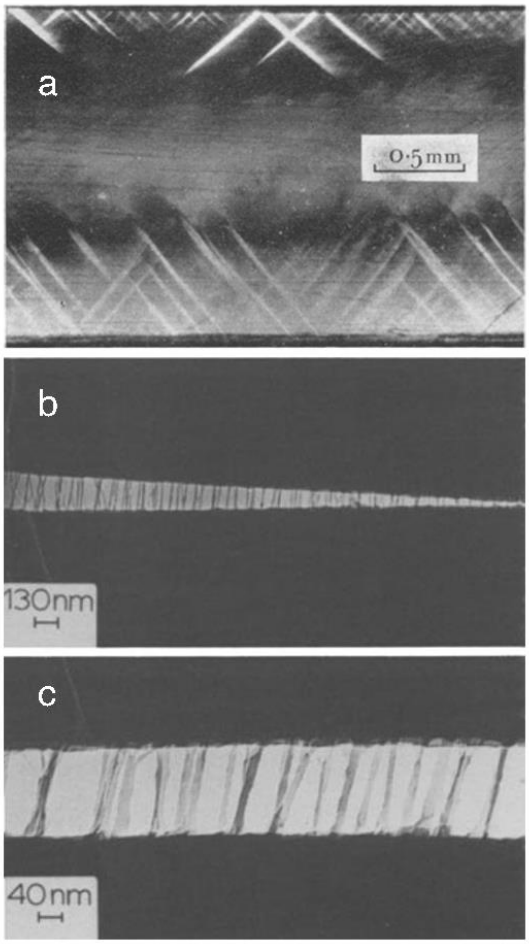

Figure 5:a) Section of a PVC sheet deformed in four points bending where shear bands are visible [4] b) and c) TEM images of crazes in PS film [5]

creation of new volume in a localized region where fibrils get oriented in the same direction of the load [5]. In Figure 5 some TEM images of shear bands and crazes are reported.

These two mechanisms are competing, and the occurrence of one instead of another depends on many factors, such as temperature, strain rate, stress state and presence of and aggressive environment. The most used criteria to characterize these two mechanisms are the modified Von Mises criterion for shear yielding and the Argon and Sternstein criteria for craze yielding [6]. Looking at Figure 6, graphs representing the stress state of a body in plane stress are reported, and the meaning of them is that

if the stress state happens to be inside the colored zone, then the body is safe, otherwise it will undergo yielding.

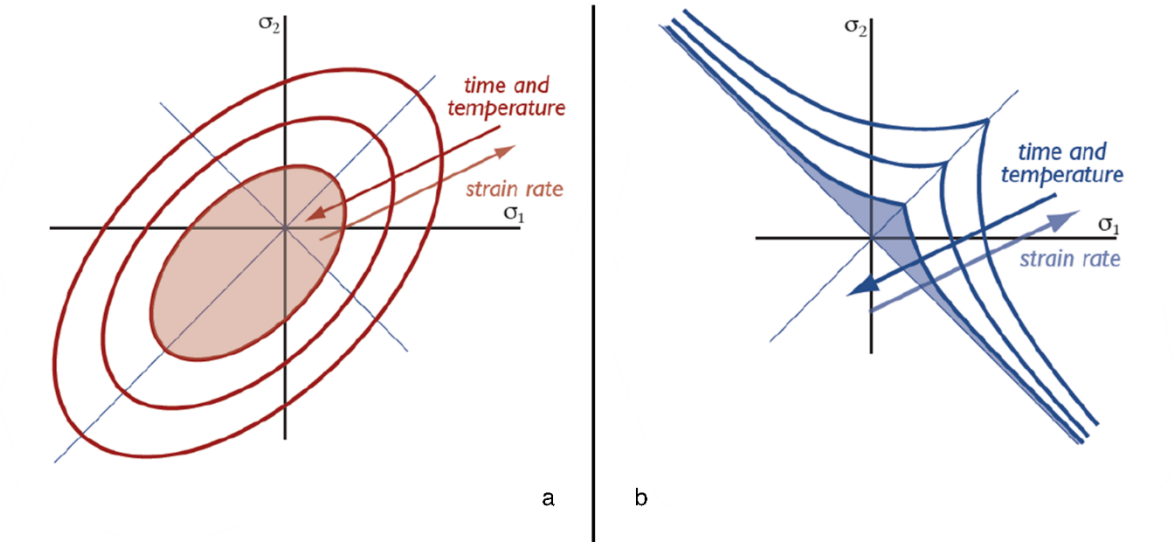

Figure 6: a) Von Mises criteria for shear yielding b) Sternstein criteria for craze yielding [6]

Another phenomenon worth mentioning in this case is cavitation. It can manifest only when a body is loaded in tension and is typical of rubber-toughened polymers, since it is a mechanism trough which toughening is achieved. The cavitation consists in the formation of a void inside a rubber particle, which then grows by elastic deformation of the particle itself. The consequence of this process is a local reduction in the bulk modulus and hydrostatic stress components. The onset of cavitation depends on the cavitation resistance of the rubber particles. If the rubbery phase is more resistant to cavitation, this process is delayed, and more elastic energy builds up in the polymeric matrix, leading to an increase in the size of the plastic zone and a higher toughness [7].

1.4.1 Crazing

This mechanism is very common among amorphous glassy polymers and will usually lead to a brittle fracture. If a tensile load is acting on a material, at a certain point near a defect the material starts developing fibrils via meniscus instability as schematized in Figure 7 [8]. This effect was observed with a TEM by Donald and Kramer (1981) [5].

According to this theory, the craze propagation front is considered to behave like a liquid, and it is not planar, but it has a wave-like shape. Upon increasing the opening

of the craze, free volume increases, and this causes molecules to flow out of the bulk and form fibrils. The high degree of molecular orientation prevents at first the rupture of the fibril. Subsequently, they can both deform by creep or be drawn from the bulk. The failure of the fibrils leads to crack initiation. In a normal fracture process, many of these events will happen simultaneously, and eventually one craze will become a crack which will propagate leading to brittle fracture.

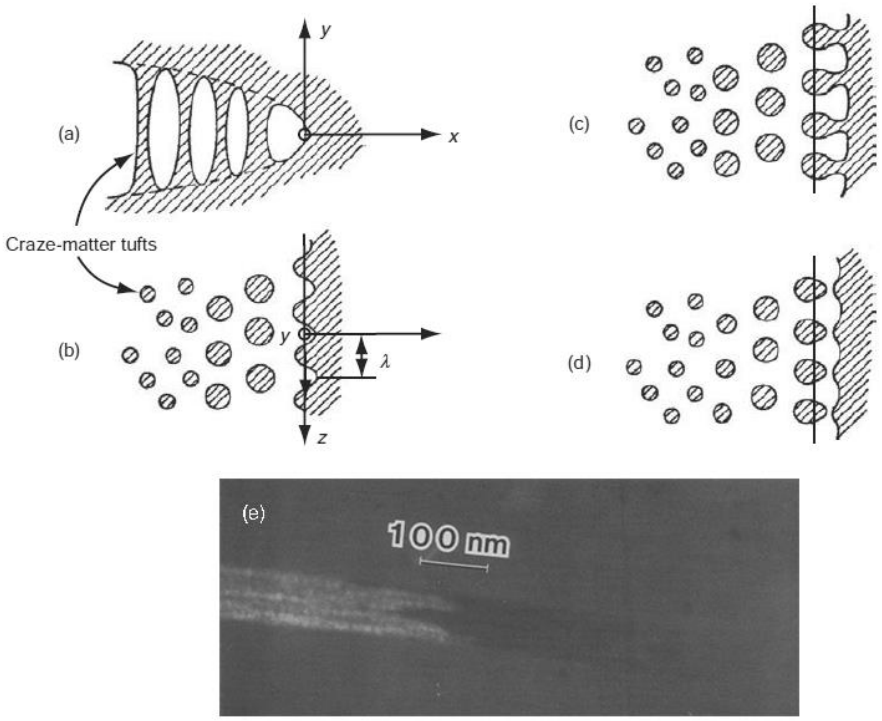

Figure 7: a) side view of the craze tip, b) top view of craze front, c) and d) advance of the craze front, e) TEM micrograph of a craze tip in poly(styrene-acrylonitrile)

The process of a craze becoming a bigger crack, however, can be assisted by the presence of a specific environment. This leads to the so-called Environmental Stress Cracking, which will be discussed section (1.5).

1.5 Environmental stress cracking

Environmental Stress Cracking (ESC) is a phenomenon due to the interaction between a polymer and a solvent which leads to a premature failure of the former. It occurs when a polymer is subjected to both a mechanical load and the contact with specific chemicals which physically interacts with it. Aggressive liquids are locally absorbed in areas subjected to high levels of stress or defects such as a craze or the tip of an

existing crack. This absorption leads to a local plasticization of the material leading to a faster fibril deformation, and so to a premature failure.

The main mechanism which causes this phenomenon is a local reduction of intermolecular forces between polymeric macromolecules, causing an increase in the rate of disentanglement. Since the process depends on the local absorption of the liquid in the region containing the crazes, ESC will manifest only if the fracture process is slow enough to allow the diffusion and absorption of the liquid, otherwise the fracture will happen as if it was not present at all. In fact, each material-active environment combination is characterized by a critical interaction time below which ESC will not affect the fracture behavior. [9] [10].

As observed in a review by [11], an estimated 15% to 25% of all failures of plastic products can be attributed to ESC, and so it is very important to measure the ESC resistance of materials which can be subjected to this phenomenon during their service life.

1.5.1 ESCR testing methods

Various testing methods have been developed during the years in order to study the interaction between a specific polymer-active environment combination. This is because, from an industrial point of view, it is important to have a ranking of the materials based on their resistance to ESC. All of these testing methods are conducted applying a load or a deformation to a specimen which is inserted in the active environment under investigation.

1.5.1.1 Bell telephone test

This method was first introduced in the Bell laboratories to evaluate the resistance to ESC of polyethylenes used for the isolations of wires and is nowadays standardized [12]. According to the procedure, rectangular-parallelepiped shaped specimens are longitudinally notched, then bent and inserted in a phial containing the active environment, as shown in Figure 8.

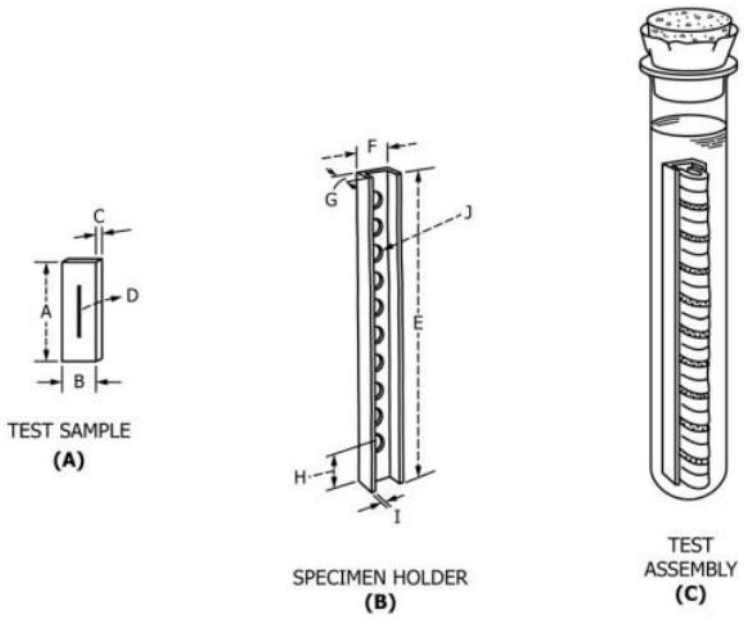

Figure 8: Bell telephone test setup scheme [12]

Then, the temperature is increased to 50°C in order to speed up the process. The result of the test can be expressed in different ways. These can be percentage of failure at the end of a specific interval, or via the F_{50} parameter, which represents the time at which N/2 specimens have failed in a test containing N specimens

Advantages of this testing method are the ease with which it can be conducted, and the fact that it can give some results in a small amount of time. However, the downsides are that the standard does not clearly define some parameters that can influence the results and the specimen geometry, the notch geometry and the concentration of the solution used as active environment are left to the operator's judgement. Also, a possible human error must be taken into account, since the failure of a specimen must be determined via visual inspection.

1.5.1.2 Bent strip method

This method is particularly fit for rigid polymers, such as HIPS, since it is very difficult to bend the specimens and insert them in the specimen holders as prescribed by the previous one. The bent strip method is standardized in ISO 22088-3 and requires that the specimen is subjected to a constant deformation using the clamping system reported in Figure 9 and is put in contact with the active environment for some time (usually 24h) at constant temperature.

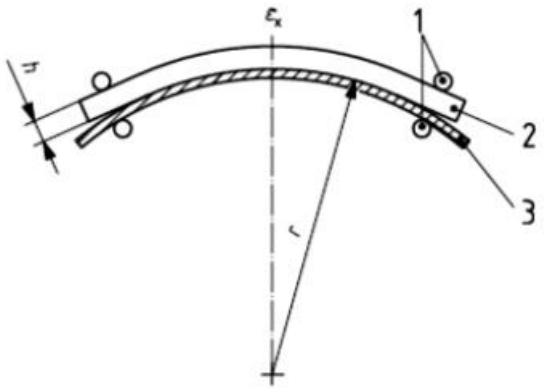

Figure 9: scheme of the clamping system for the bent-strip method test [[43]

After 24h, some crazes will be ideally present on the specimen, and the latter can then be tested. The chosen testing method is not standardized, it can be for example tension or bending, and the final result will be the comparison between a property measured on the specimen exposed to the active environment and on an unexposed one.

1.6 Fracture mechanics

Fracture mechanics is the study of the influence of loading, crack size, and structural geometry on the fracture resistance of materials containing natural flaws and cracks [13]. The first research in the field of Linear Elastic Fracture Mechanics (LEFM) were conducted in 1898 by the German engineer Ernst Gustav Kirsch. He developed a linear elastic solution for stresses around a hole in an infinite plate, named Kirsch's equations [14]. The next step was taken by the British engineer Charles Inglis, who conducted a similar analysis to the one done by Kirsch, but for the case of an elliptical crack of varying aspect ratio, which taken as a limit case can represent a sharp crack [15]. Then, in the year 1921, Griffith published a study where he applied Inglis' stress analysis of an elliptical hole to the unstable propagation of a crack. He invoked the First Law of

Thermodynamics and developed a fracture theory based on an energy balance [16]. According to this, a flaw becomes unstable, causing fracture, when the strain energy release caused by the growth of a crack overcomes the surface energy of the material. This approach turned out to suit particularly well the case of glass (a brittle material), but not metals. During the following years there would not be any major contribution to the development of LEFM, until the research in the subject resumed due to what happened to the Liberty ships during World War II. They were a series of vessels supplied by the United States to Great Britain, built following a revolutionary procedure which allowed them to be ready much faster than before. They seemed like an engineering success, up until 1943 when 400 among roughly 2700 of them suffered fracture. In 20 of them the fracture was total, meaning that they essentially broke in half as shown in Figure 10.

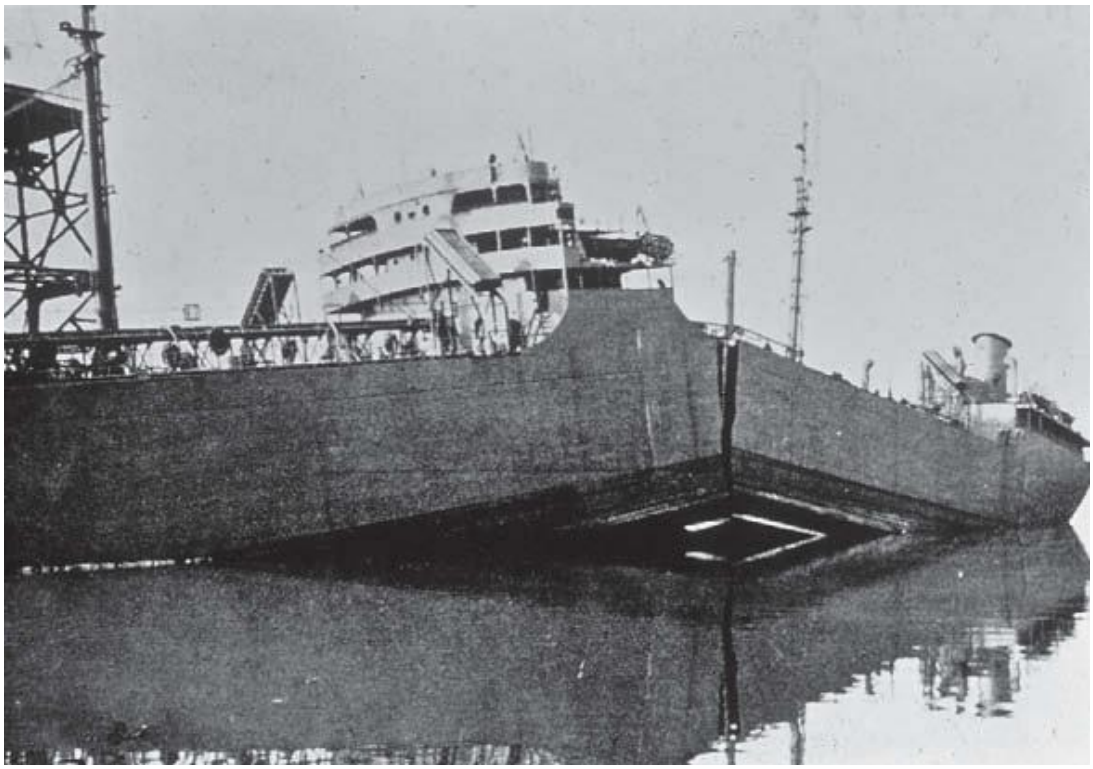

Figure 10: fracture of the "Schenectady" Liberty ship, 1943 [45]

After this event, the Naval Research Laboratory established a research group led by Dr. G. R. Irwin. His initial contribution was to modify Griffith's theory from years before, by adding a term in the equation accounting for the energy dissipated by local plastic flow [17]. Subsequently, Irwin developed the energy release rate concept [18], and then picked up a paper of years before by Westergaard [19] and used its approach to show that stress and displacement near the crack tip could be described by a

parameter, which was related to the energy release rate, and this parameter will be later known as the stress intensity factor [20]. Also, in the same years Williams derived in a different way some crack tips solutions which were essentially the same as Irwin ones [21]. In the years 1960-61, many studies on the topic of crack tip plasticity were published. This is important since LEFM loses in validity once large scale yielding accompanies failure. Irwin proposed a relatively simple correction to the previous LEFM [22], while Dugdale and Barenblatt developed more complicated models [23]. Wells proposed as an alternative fracture criterion the crack tip opening displacement (CTOD) [24]. In 1968 Rice was able to generalize the concept of energy release rate to nonlinear materials with the use of a line integral, called the J integral [25]. The application of these concepts to design was made possible not before 1976 when Shih and Hutchinson provided the theoretical framework for the application of fracture mechanics to material design [26]. Finally, Shih demonstrated a relationship between the J integral and CTOD, showing that they are both equally valid to characterize fracture [27].

1.7 LEFM

Irwin proposed an approach to fracture mechanics which is essentially the same proposed by Griffith, but it is more convenient to solve engineering problems. He defined an energy release rate parameter G, which is a measure of the energy available for an increment of the area of the defect (dA):

$$G = -\frac{d\Pi}{dA} \tag{1-5}$$

where Π is the potential energy supplied by the internal strain energy and external forces. So, according to Griffith's considerations, it can be demonstrated that G can be written as:

$$G = \frac{\pi\sigma^2 a}{E} \tag{1-6}$$

where σ is the stress applied, a is the crack length and E is the Young's modulus. Crack extension occurs when G reaches a critical value, G_c:

$$G_c = \frac{dW_s}{dA} = 2w_f \tag{1-7}$$

where W_s is the work required to create new surfaces and w_f is the fracture energy which includes, depending on the material, plastic, viscoelastic or viscoplastic effects.

Considering a cracked plate of thickness B, it can be demonstrated that we can express the energy release rate as proposed by Kies and Irwin [27]:

$$G = \frac{P^2}{2B}\frac{dC}{da} = \frac{U_s}{B}\frac{1}{C}\frac{dC}{da} \tag{1-8}$$

where C is the material compliance and is defined as the reciprocal of the stiffness:

$$C = \frac{\Delta}{P} \tag{1-9}$$

where P is the load applied to the plate and Δ the corresponding displacement. Also, the energy release rate is the same for both the cases of load control and displacement control. We can finally introduce in equation (1-6) the width W of the body and find the expression:

$$G = \frac{U_s}{BW}\frac{1}{C}\frac{dC}{d\left(\frac{a}{W}\right)} = \frac{U_s}{BW}\frac{1}{\psi\left(\frac{a}{W}\right)} \tag{1-10}$$

Where $\psi\left(\frac{a}{W}\right)$ is an energy calibration factor, whose value depends on the test configuration.

The same approach can be taken to derive another fracture parameter: K. To do this, only mode I crack loading will be taken into account (Figure 11) and a polar coordinate system centered on the crack tip will be introduced as shown in Figure 12.

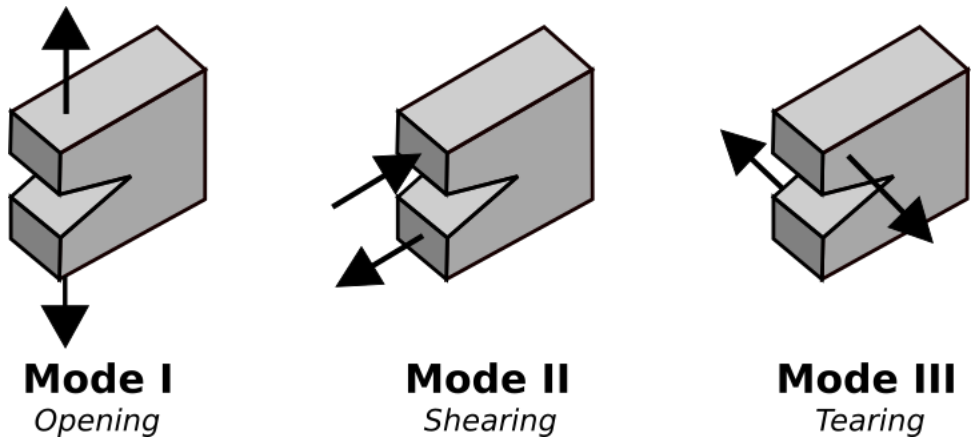

Figure 11: Crack loading modes

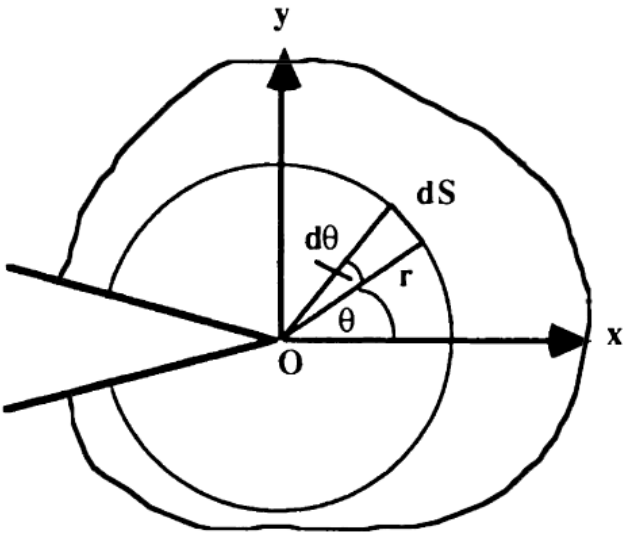

Figure 12: scheme of the used polar coordinate system

With respect to this coordinate system, the stress field at crack tip can be expressed as:

$$\sigma_{ij} = \frac{K_I}{\sqrt{2\pi r}} f_{ij}(\theta) \tag{1-11}$$

Where K_I is the stress intensity factor for mode I crack loading and f_{ij} is a dimensionless function of θ. Stresses in the x and y directions are equal, and can be expressed as:

$$\sigma_{xx} = \sigma_{yy} = \frac{K_I}{\sqrt{2\pi r}} \tag{1-12}$$

This equation is valid only near the crack tip, where the stress field is governed by the $\frac{1}{\sqrt{r}}$ singularity. According to (Equation 1-12) the elastic stresses would reach an infinite value at exactly the crack tip. This of course is not the case, since non-linearity must be taken into account, in particular the yielding of the region around the crack tip. The condition for LEFM to be applicable is that the size of this plastically deformed zone must be limited with respect to the characteristic dimensions of the body (small scale yielding condition). Far from the crack tip, stresses are governed by boundary conditions. The stress intensity factor defines the amplitude of the crack tip singularity, where stresses increase in proportion with K. Another important concept is that K completely defines the stress, strain and displacement states as a function of r and θ. However, to make practical use of the stress intensity factor, it is important to be able to determine it by knowing the remote loads and geometry. There are many

solutions to this problem for simpler geometries, or they can be derived numerically for more complex ones. They are in the form:

$$K = Y\sigma\sqrt{\pi a} \tag{1-13}$$

where Y is the shape factor for the considered geometry and σ the stress applied at the boundary. As said previously, these approaches are equivalent and K and G can be linked by the expression:

$$G = \frac{K^2}{E'} \tag{1-14}$$

where $E' = E$ in plane stress state and $E' = \frac{E}{1-\nu^2}$ in plane strain conditions, E being the Young's modulus and ν the Poisson's ratio of the material.

The dimensions of the plastic zone can be evaluated by means of two different approaches, one proposed by Irwin (Equation 1-15) where the plastic zone is considered of circular shape, and one by Dugdale (Equation 1-16) with a slender and elongated plastics zone, both valid in plane stress condition:

$$r_p = \frac{1}{\pi}\left(\frac{K_I}{\sigma_y}\right)^2 \tag{1-15}$$

$$r_p = \frac{\pi}{8}\left(\frac{K_I}{\sigma_y}\right)^2 \tag{1-16}$$

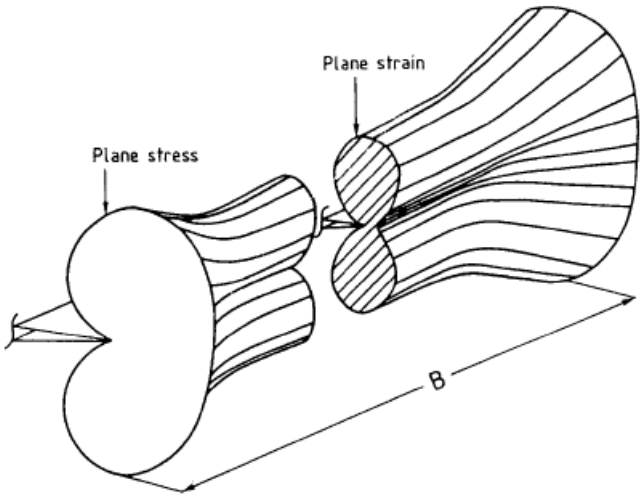

Figure 13: Shape of the plastic zone at crack tip [44]

Plastic deformations are a dissipative mechanism, and so relate to the material resistance to crack growth. Since in plane stress condition the plastic zone is larger, K_{IC} will be higher then in plane strain condition. In a real body, we must consider a combination of these 2 mechanisms, but for increasing dimensions of the body the plane strain contribution becomes predominant, since it is characteristic of the bulk of the material. In a large enough body, a limit value for K_{IC} will be eventually reached, and this value can be considered as intrinsic of the material.

According to ISO 13586, specimen used to determine K_{IC} must satisfy some dimensional requirements, in particular:

$$B, a, W - a, h \geq 2.5 \left(\frac{K}{\sigma_y}\right)^2 \tag{1-17}$$

where the condition of the thickness has the aim to ensure plane strain condition, and the others that the plastic zone is small compared to the specimen dimension.

1.8 Viscoelastic fracture mechanics

The LEFM theory discussed up to this point takes as an assumption that the bulk of the material can be considered as linear elastic. This is not the case of polymers, however, as they behave as viscoelastic materials, and so their fracture behavior is also time-dependent. This usually happens as a consequence of a slow crack propagation, which originates from a defect by means of a mechanical stress. According to a theory proposed by Williams, under the assumptions of a linear and only slightly viscoelastic behavior, equations developed in the LEFM theory can be employed simply replacing some constant material properties with the corresponding time-dependent quantities: this is called pseudo-elastic approach. In this framework, fracture toughness can be expressed as:

$$G_{IC} = \delta_c \sigma_y(t) \tag{1-18}$$

where δ_c is the crack tip opening displacement, which here is assumed to be constant during the time window considered. It is also known that, in polymers, crack initiation will occur after an initiation time t_i. If we then express the yield stress time dependence with a power law, we get:

$$G_{IC}(t_i) = \delta_C \sigma_y(t_i) = \delta_C \sigma_{y0} t_i^{-m} \tag{1-19}$$

To get more information also on crack propagation we can start inserting equation (1-14) into the expression of the plastic zone by Dugdale in plane strain condition (equation (1-16)):

$$r_p = \frac{\pi}{3 \cdot 8}\left(\frac{K_{IC}}{\sigma_y}\right)^2 = \frac{\pi}{24}\frac{G_{IC} \cdot E(t)}{(1-\nu^2) \cdot \sigma_y^2(t)} = \frac{\pi}{24}\frac{\delta_C \cdot E(t)}{(1-\nu^2) \cdot \sigma_y(t)} \tag{1-20}$$

and considering a power law time-dependence also for E it can be written as:

$$r_p = \frac{\pi}{24}\frac{\delta_C \cdot E_0 t^{-n}}{(1-\nu^2) \cdot \sigma_{y0} t^{-m}} = \frac{\pi}{24}\frac{\delta_C \cdot E_0}{(1-\nu^2) \cdot \sigma_{y0}} \cdot t^{-n+m} \tag{1-21}$$

then, considering a crack moving at constant speed $\dot{a}$, the time needed to cross the process zone is:

$$t = \frac{r_p}{\dot{a}} \tag{1-22}$$

Substituting (Equation 1-20) into (Equation 1-19) we find:

$$G_{IC} = \delta_c \sigma_{y0} \cdot \left(\frac{\pi}{24}\frac{\delta_C \cdot E_0}{(1-\nu^2) \cdot \sigma_{y0}}\right)^{-\frac{m}{1+n-m}} \cdot \dot{a}^{\frac{m}{1+n-m}} \tag{1-23}$$

and finally, exploiting again the relations in (Equation 1-14), we obtain:

$$K_{IC} = \left(\delta_C \sigma_{y0} E_0\right)^{\frac{1}{2}} \cdot t_i^{-\frac{n+m}{2}} \tag{1-24}$$

which links K_{IC} to the initiation time and

$$K_{IC} = \left(\delta_c \sigma_{y0} E_0\right)^{\frac{1}{2}} \cdot \left(\frac{\pi}{24}\frac{\delta_C \cdot E_0}{(1-\nu^2) \cdot \sigma_{y0}}\right)^{-\frac{n+m}{2(1+n-m)}} \cdot \dot{a}^{\frac{n+m}{2(1+n-m)}} \tag{1-25}$$

linking K_{IC} to the crack speed. To sum up, these equations predict a power law dependence between G_{IC} and t_i or $\dot{a}$, and that the exponents of these power laws depend on the relaxation modulus and on the yield stress.

Independently from the chosen fracture parameter, the failure time can be expressed as:

$$t_f = t_i + t_p \tag{1-26}$$

where t_p is the time required by the crack to propagate and cause the failure of the material. By considering K as the relevant fracture parameter, (Equations 1-24) and (Equation 1-25) can be written in a more compact form as:

$$t_i = A \cdot K_{IC,0}^n \tag{1-27}$$

$$\dot{a} = B \cdot K_{IC}^m \tag{1-28}$$

then, (Equation 1-26) can be rewritten as:

$$t_f = A \cdot K_{IC,0}^n + \int_{a_0}^{a_f} \frac{da}{B \cdot K_{IC}^m} \tag{1-29}$$

where A, B, n and m are constants, $K_{IC,0}$ is the critical stress intensity factor at crack initiation and a_0 and a_f are the initial and final crack length, respectively. This approach is very interesting from an engineering point of view, since by means of it, by knowing the body geometry and the boundary conditions, the failure time of any component can be analytically predicted.

1.9 Fracture mechanics approach to ESC

Here, some of the main studies to this matter will be reported. The first steps in understanding ESC through LEFM were taken by Williams and Marshall in 1975 [28]. The main result of this study was the definition of different regimes of crack growth rate (Figure 14).

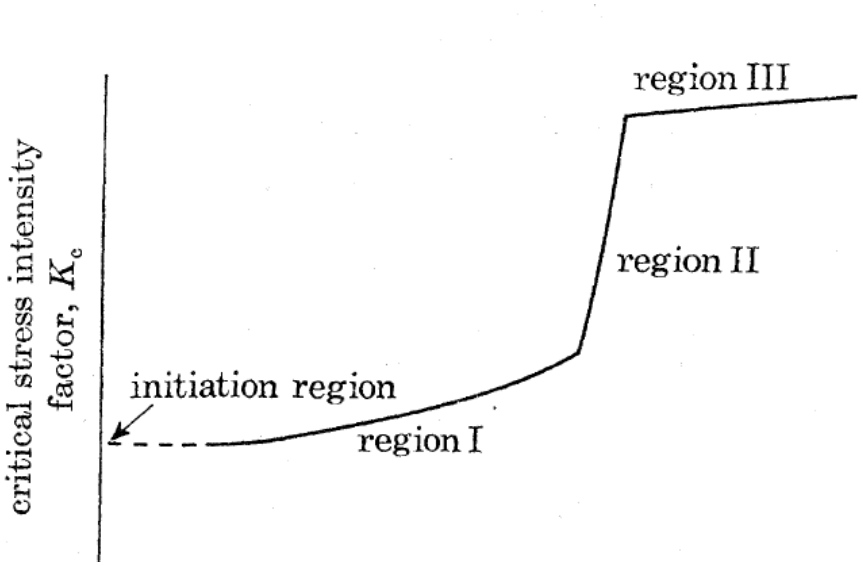

Figure 14: schematization of crack speed effect on toughness [28]

What is important in this graph is that if a crack is propagating at slow speed (region I), the environment has time to penetrate in it and affect the toughness of the material. On the other hand, if the crack propagates fast enough (region III), the environment is unable to affect the material's toughness which turns out to be the same as it would be without the presence of the active environment. This introduced the concept of the critical interaction time, which will be defined later. Then, in 1983, Chan and Williams proposed a study where LEFM was applied to study the behavior of HDPE in distilled water and in an aqueous detergent solution, testing SENB specimens in 3-point bending. The main result was a K_c vs $\dot{a}$ curve reported in Figure 15, which demonstrated that it is possible to use LEFM to characterize this material [29].

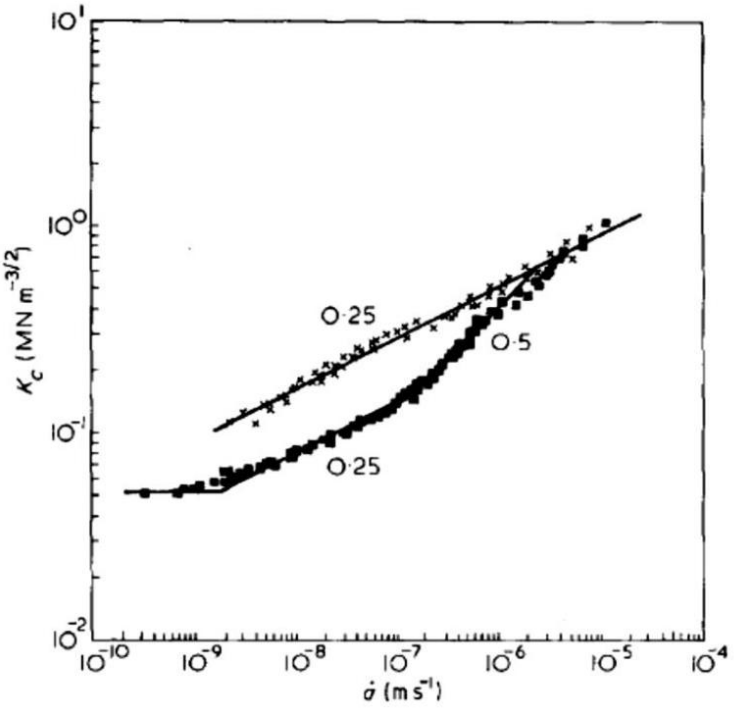

Figure 15: Critical toughness vs. crack speed in distilled water (crosses) and in a detergent (squares)

A similar result was obtained in the same years by Tonyali and Brown [30], who were able to obtain again an unique K_c vs $\dot{a}$ curve on LDPE using specimens with different dimensions and different testing configurations.

Then, in 2003, Rink et al. [31] conducted a study again on polyethylene, performing four-point bending creep tests, detecting crack initiation via a compliance calibration method and studying the effect of the active environment on this phase of fracture. One of the main takeaways of this work was the fact that the environment affected the resistance of the polymer only below a critical stress intensity factor, K_{IC}^*.

Another approach to this matter was taken by Alstaedt in 2004 [32] by conducting fatigue tests on HIPS in sunflower oil and polycarbonate in fatty acid emulsion. In this work the influence of molecular weight, material orientation and rubber particle introduction on the ESC resistance of HIPS was evaluated.

The combination HIPS-sunflower oil and HDPE-detergents was further investigated by Andena et al. [33], who pointed out that it was possible to find unique K_c vs t_i and K vs $\dot{a}$ curves using different testing configurations and loading histories. Later, the same authors investigated on the effect of processing on the ESC resistance of HIPS [34]. In 2016, Kamaludin et al. [35] [36] studied the ESC of 4 different polymer-active environment combinations using G as fracture parameter for both crack initiation and propagation. They proposed the use of a parameter λ for the evaluation of the effect of the active environment on the fracture resistance of polymers:

$$\lambda = \frac{t_i^*}{t_{i,\max}} \cdot \frac{\dot{a}_{\min}}{\dot{a}^*} \tag{1-30}$$

where t_i^* and $\dot{a}^*$ are the critical interaction time and crack speed and $t_{i,\max}$ and $\dot{a}_{\min}$ are the maximum value of initiation time and minimum crack growth rate measured in a chosen experimental window. This is considered as the material sensitivity to ESC, approaching zero for material with low ESC resistance and to 1 for ESC resistant materials.

In the last years, Contino et al. [37] progressed further on the study of HDPE. They first confirmed that it was possible to apply LEFM to this material considering both K and G as a fracture parameter, and that these two approaches were equivalent in individuating the critical interaction times and crack growth rate, even if HDPE behaves non-linearly and the pseudo-elastic approach was used. This is not trivial since the passage from K to G and vice versa is computed by Equation 1-14 where the modulus must be taken for a specified value of time. Finally, in [38], the applicability of the time-temperature superposition postulate was investigated on the fracture data again on HDPE, and it turned out that it was possible to build master curves for K_c vs t_i and K vs $\dot{a}$ data. This is important since by doing so it is possible to perform tests at high temperature and extrapolate the obtained data at the desired temperature to make predictions. More on this will be explained in the following section. Moreover, this study highlighted the fact that the temperature influences the results only because of the inherent viscoelasticity of the polymers, and not by changing the mechanism of interaction between the material and the active environment, at least in the range investigated.

2 Experimental details

2.1 Specimen preparation

The materials used in this work are two different HIPS grades:

- HIPS 1: a grade specifically designed to be more resistant to ESC, result achieved with a larger size of the rubber particles [39].
- HIPS 2: a general-purpose grade.

These were kindly supplied by ENI Versalis in form of pellets. Properties of these 2 materials are reported in Table 1. The selected active environment of choice was sunflower oil (Carapelli Giglio oro), already considered in previous studies highlighting the interaction between HIPS and this oil [40].

Table 1: Properties of the 2 HIPS grades from technical sheets

Property	**Conditions**	**Normative**	**Units**	**Materials**	
				1	2
Density		ISO 1183	g/cm^3	1.04	1.04
Melt flow rate	200°C-5Kg	ISO1183	g/10 min	3	4
T_g	DMA 1Hz, 1°C/min		°C	108	110
Yield stress	50mm/min		MPa	16	21
Break stress	50mm/min	ISO527	MPa	23.5	24
Break strain	50mm/min		%	70	60
Modulus	1mm/min		MPa	1450	1850
Flexural strength	2mm/min	ISO178	MPa	35	38

Plates of these materials were prepared by applying to the pellets a compression molding cycle, followed by a thermal treatment aiming at reducing the internal stresses produced during the molding [9]. The optimal combination of time, temperature and pressure applied had already been investigated in previous studies [40]. After plates have been produced, they must then be machined to obtain the desired geometry.

2.1.1 Compression molding

The output plates had a surface area of 170x200mm (as imposed by the dimensions of the available mold), and a nominal thickness of 6mm.

The applied compression molding cycle was the following, as depicted in Figure 16:

- Mold was preheated at 200°C
- Pellets were inserted in the mold, which is then closed with no pressure applied
- Pellets were left to heat up for 10 minutes
- A pressure of 2MPa was applied for 6-7 minutes to compact pellets and expel air
- The applied pressure was increased to 4MPa for 8 minutes
- Pressure was released by simply cooling down to 140°C using the water cooling
- A slow cooling from 140°C to 100°C is achieved by simply turning off the water cooling and leaving the system as it is for approximately 20 minutes. This was done to ensure a controlled cooling at the T_g of the material.
- A final fast cooling to room temperature was achieved using the water cooling system.

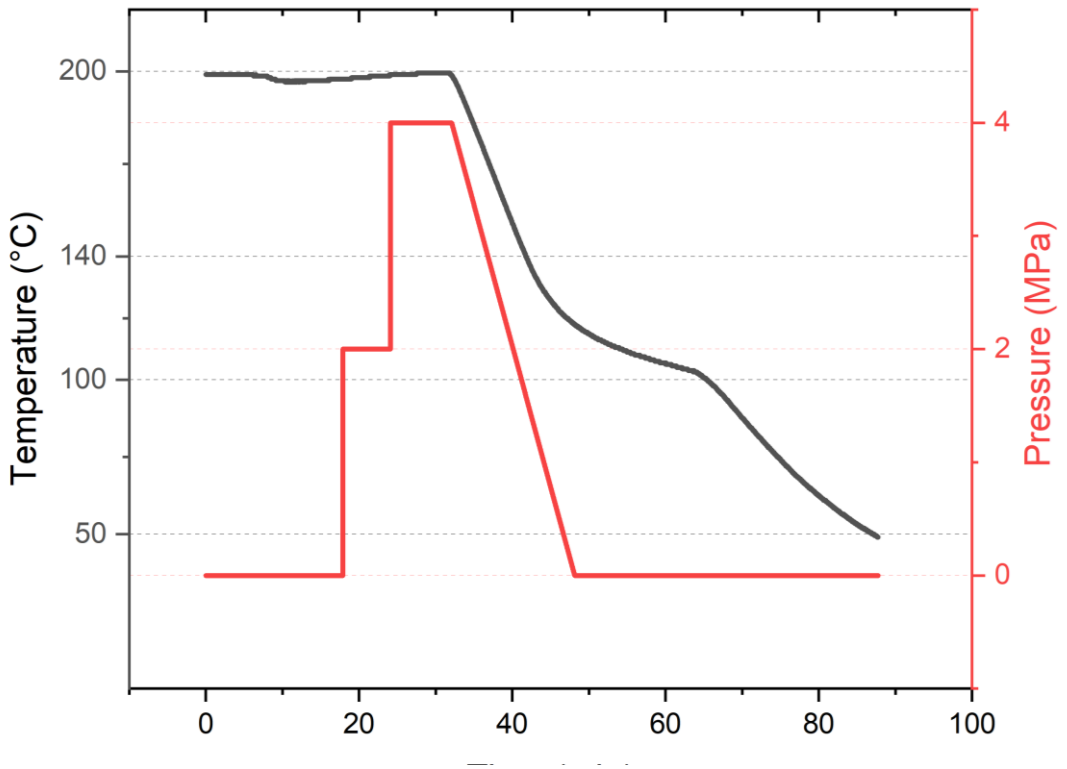

Figure 16: Temperature and pressure vs. time in the compression molding cycle

During the cooling steps, the temperature of the male and of the female molds were monitored using two thermocouples, to verify uniformity of cooling, thus minimizing the generated internal stresses.

To further mitigate the effect of possible internal stresses and other inhomogeneities related to the compression molding process, the obtained plates were placed in an oven and subjected to the following thermal treatment, depicted in Figure 17:thermal treatment:

- heating from room temperature to 90°C in 30 minutes
- temperature maintained constant at 90°C, which is just below the T_g of the material, for 1 hour.
- very slow cooling to room temperature in 10 hours

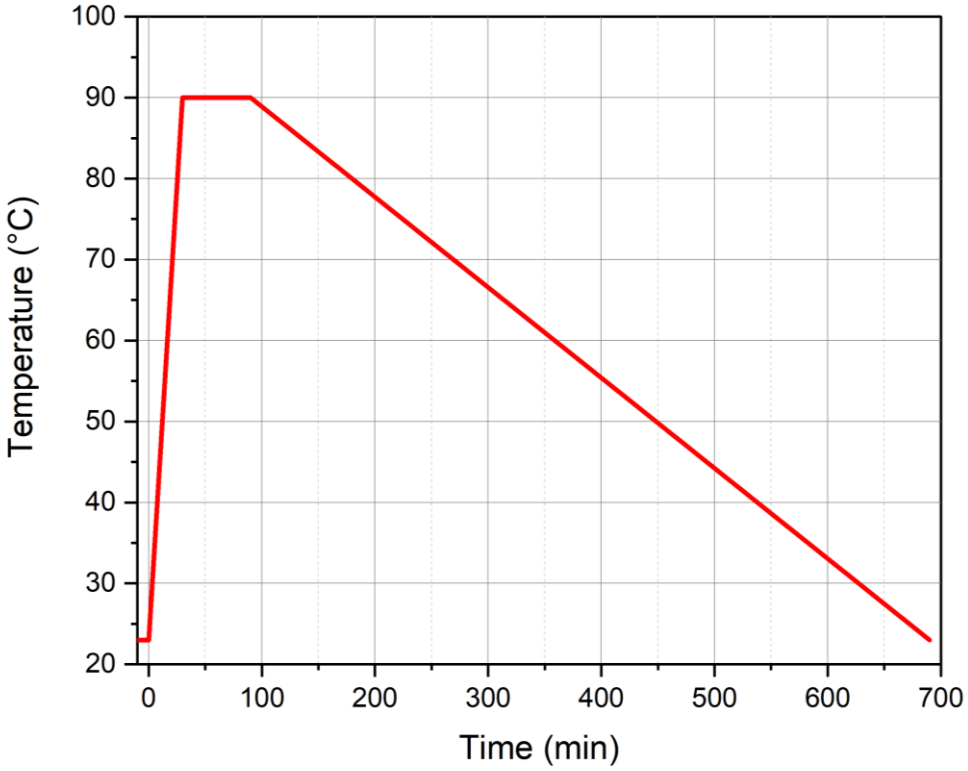

Figure 17:thermal treatment

2.1.2 SEN(B) Specimen machining

After the sheets have been molded, they were machined in order to obtain the specimen of the desired dimensions. Mostly fracture tests have been performed, and they have been conducted in bending, both at constant load (creep) and at constant displacement rate. The adopted specimen geometry was the same for all of the tests performed in bending, the so-called SENB geometry (Single Edged Notched Bending) depicted in Figure 18. The dimensions were, however, slightly different between the two testing configurations, mainly in order to satisfy some constraints imposed by the testing equipment. These dimensions are reported in Figure 18 and are in accordance with ISO 13856. Also, different types of specimens were prepared for the creep configuration. Most of them were produced with a sharp notch from which fracture can initiate, and a few of them were produced with a blunt notch, so that fracture would not initiate during the considered testing time. This was important to obtain

information about the specimen compliance excluding the contribution given by the crack, but this aspect will be better explained in the next chapter.

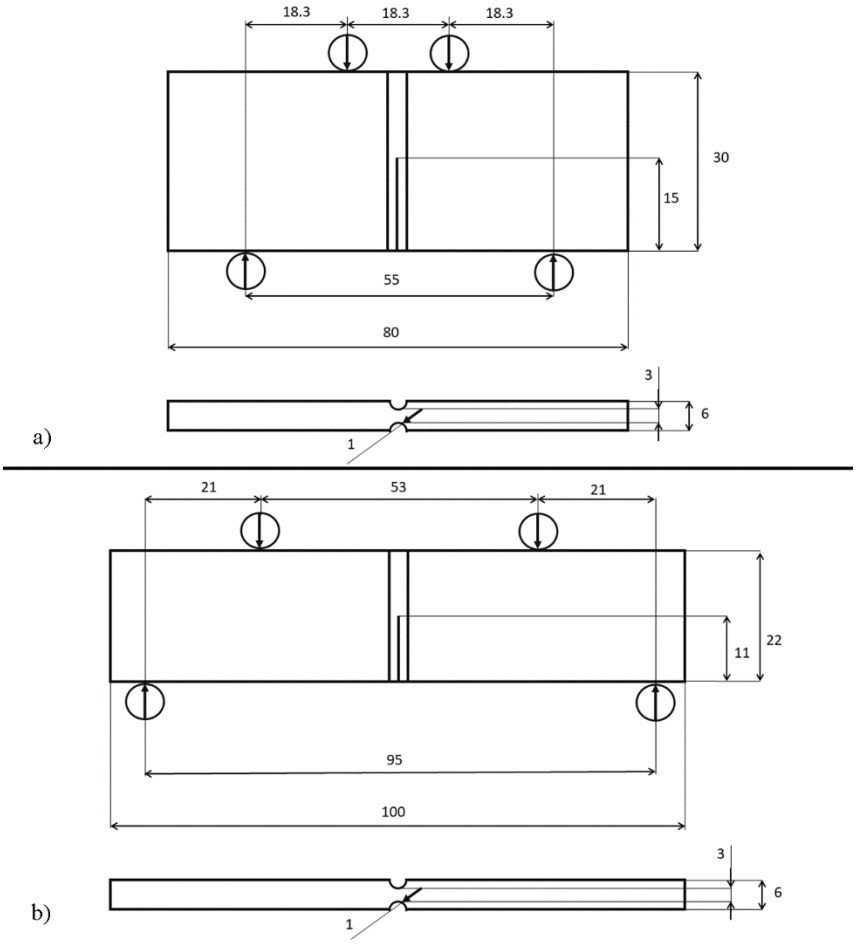

Figure 18: SEN(B) specimen in four-point bending configurations, a) creep b) constant displacement rate (measures in mm)

The proportions between the upper and lower pins distances changes: in creep the distance between the upper pins is 0.33 times the one of the lower pins, in constant displacement rate is 0.56 the one of the lower pins. To obtain the specified geometry starting from a sheet of material, roughly square bars were cut from the plates, using a band saw. They were then brought to the desired dimensions with a milling machine equipped with a helical blade, with a cutting depth of 0.5mm. A sharp notch was hence introduced in most of the specimens via automated "chisel-wise" cutting, obtaining a final notch root radius lower than 10 μm. As previously reported, in some of the specimens a blunt notch was introduced: this operation was conducted using a

diamond-studded circular blade having a radius of 1mm. Finally, grooves were introduced with the same blade used for blunt notching in both types of specimens.

The dimensions reported in Table 2 were chosen not only to satisfy some geometrical constraints imposed by the testing equipment, but also other conditions. In particular:

- The dimension of the plastic zone must be small compared to the specimen width (W), which requires a ligament size of at least 10mm as found by [40], which indicates that the plastic zone developed in this material is quite big.
- The plane strain condition must be satisfied, which requires a thickness (B) of at least 5mm.

These are essential in order to be able to define the characterize the stress intensity factors as an intrinsic property of the material, independent from the geometry and dimensions of the specimens.

2.2 Testing methods

2.2.1 Creep tests

All creep tests were conducted on 3 custom built testing machines, which allow to perform tests in the 4-point bending configuration. These machines consist in a fixed part, which accommodates the 2 lower pins, at a fixed distance of 55mm. The 2 upper pins are part of the movable part of the machine, which is attached to a hollow cylinder that can be filled with lead spheres to reach the desired weight for the test. By filling the cylinder, it is possible to reach a weight of about 16kg but putting on top of it some additional lead weight it is possible to reach a much higher value of weight, up to about 35Kg This cylinder is kept suspended by a pneumatic system when the specimen is being loaded in the machine and can be released as a dead weight in about 5 seconds. A limit of this setup is that the application of the load is not instantaneous, so if the tests were too fast (faster than about 10 times the time needed for the weight to be applied), they could not be considered valid since the condition of pure creep was not satisfied.

This configuration is able to apply on the specimen a constant bending moment in the region between the two upper pins. This produces a displacement in this region that is measured by the use of some linear variable displacement transducers (LVDTs) and registered in a .txt file containing displacement data coupled with the time of the experiment.

Before starting the test, it is important to position the specimen inside the machine, put the upper pins in contact with it (without releasing the dead weight) and record the

reading of the LVDT. This is important because later, when analyzing the data, this value of the displacement will be taken as the reference value at which the test effectively started. The LVDTs were not put directly in contact with the specimen, but with a metal plate of known thickness on top of the movable part of the machine, as shown in Figure 20. This was done because doing so the tip of the LVDT was always in contact with a straight surface, avoiding the risk of bad readings caused by misplacement of the specimen.

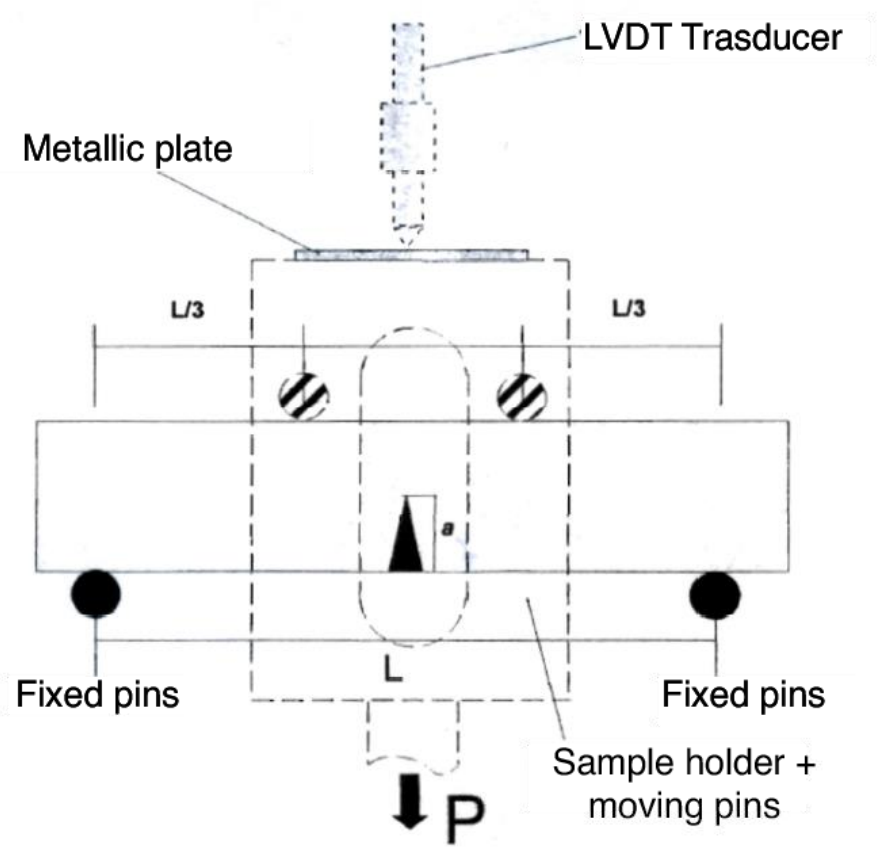

Figure 19: scheme of the configuration of the creep machines [40]

This apparatus is inserted in a thermostatic chamber with two radiative panels and fans to control the temperature inside the chamber, which is monitored via a built-in thermocouple. With this configuration, visual observation of the crack is not possible. Tests were performed with various loads ranging from 20N to 280N, depending on the desired value of stress intensity factor. The tested temperatures were 31°C (the lowest one which can be effectively controlled by the machine, which is not equipped with a cooling unit), 40°C and 50°C.

For the tests to be conducted in active environment, specimens have been put inside a thin polyethylene bag filled with sunflower oil, as shown in Figure 21. The active environment must be enough to ensure the contact with the specimen for the whole duration of the test, but not too much in order to avoid piercing the bag when inserting the specimen in the machines.

Figure 20: bag used to conduct creep tests in active environment

2.2.2 Constant displacement rate bending tests

Tests were performed on an Instron5967 electro-mechanical dynamometer equipped with a 2kN load cell, measuring the deflection of the sample from the displacement of the crosshead. The testing configuration is again 4-point bending, with a different distance between the pins as indicated in section 2.1.2. The machine is operating in a thermostatic room, with a controlled temperature of 23°C, and almost all tests were conducted at that temperature. Some tests were conducted also at 31°C and 40°C, using an oven able to fit in the dynamometer Various displacement rates were used, ranging from 0.0001mm/min to 10mm/min. Tests at high displacement rate in a range that could not be performed in creep were performed, together with some in an overlapping range.

During the test, it is possible to visually monitor in real time and record the progression of the crack, as shown in Figure 22.

Figure 21: frame extracted from a recording of a test

This was done using a 10 Megapixel uEye UI5490 SE camera equipped with different macro lenses for relatively quick tests (with a displacement rate greater than 0.001 mm/min). The frame rate was variable and was changed according to the speed of the test, ranging from 20 to 1 fps (frame per second). For longer tests, a slightly different setup was used: a Canon Reflex camera with the same optical setup was employed

Figure 22: tank setup used for tests in active environment

together with a timelapse software. This was done since these tests were very slow and so were performed leaving the machine operating overnight, and by doing so it was possible to acquire a frame each 20 seconds. In any case, the data acquisition frequency of the dynamometer was synchronized with the one of the video recordings.For test conducted in the active environment, a custom-built tank was attached to the dynamometer, as shown in Figure 23. The tank contains about 5 liters of liquids, so to limit the use of oil it was initially filled with water, and subsequently with oil. Being oil less dense than water, it remains located in the upper region, where the specimen is present. The tank presents a front glass window to allow visual inspection.

3 Data analysis

3.1 Creep tests

The material behavior was characterized by analyzing the initiation time for fracture and the crack propagation speed. The aim was to obtain for each material K vs. t_i, K vs. $\dot{a}$, G vs t_i and G vs $\dot{a}$ curves.

3.1.1 Stress intensity factor

For the four-point bending configuration, the stress intensity factor can be written, as reported in [41], as:

$$K = Y\left(\frac{a}{W}\right)\frac{6M\sqrt{\pi a}}{W^2} \tag{3-1}$$

where Y is the shape factor, which is valid when the condition $\frac{a}{W} \leq 0.6$ is satisfied, and is expressed as:

$$Y = 1.12 - 1.39\left(\frac{a}{W}\right) + 7.32\left(\frac{a}{W}\right)^2 - 13.1\left(\frac{a}{W}\right)^3 + 14\left(\frac{a}{W}\right)^4 \tag{3-2}$$

and M is the bending moment for unit thickness, which can be written:

$$M = \frac{PL}{6B^*} \tag{3-3}$$

Also, B^* is not the actual thickness of the specimen but represents a correction to it needed because of the presence of the groove. It can be written, according to [9], as:

$$B^* = B^{0.263} B_g^{0.737} \tag{3-4}$$

where B_g is the thickness in the region of the groove. This gives a final expression for the stress intensity factor as:

$$K = Y\left(\frac{a}{W}\right)\frac{PL\sqrt{\pi a}}{B^* W^2} \tag{3-5}$$

3.1.2 Energy release rate

In the four-point bending configuration, G can be determined using equation 1-6, given P is known and constant and $\frac{dC}{da}$ can be determined easily according to section 3.1.2. This, however, was not a good approach because of the noisiness of the experimental data. The alternative was to apply equation 1-8, which in this case becomes:

$$G = \frac{U}{BW} \cdot \frac{1}{\psi_{FPB}\left(\frac{a}{W}\right)} \tag{3-6}$$

where U is the energy accumulated by the specimen up to initiation (or up to the considered time) and ψ_{FPB} is the energy calibration factor for the four-point bending configuration (see Appendix X). U is in the case of creep test computed as:

$$U = P \cdot \delta \tag{3-7}$$

where δ is the displacement recorded by the LVDT at a given time.

3.1.3 Initiation time and crack speed evaluation

Since, as previously anticipated, visual observation of the crack was not possible due to the geometry of the testing equipment, an alternative method based on the specimen's compliance has been used. This method allows to determine crack initiation and crack growth rate from the displacement output of the LVDTs in the creep machines. This method has already been used for the same purpose in other studies [9] [42]. As explained in chapter 1, we have the relation:

$$\frac{dC}{da} = \frac{2B}{P^2 E} K^2 \tag{3-8}$$

and combining Equations (3-5) and (3-6) we find:

$$\frac{dC}{da} = \frac{2B}{P^2E}\left[Y\left(\frac{a}{W}\right)\frac{PL\sqrt{\pi a}}{BW^2}\right]^2 = \frac{2L^2\pi}{EBW^4}aY^2\left(\frac{a}{W}\right) \tag{3-9}$$

and integrating:

$$C\left(\frac{a}{W}\right) = C_0 + \frac{2\pi L^2}{EBW^2}\int_o^{\frac{\bar{a}}{W}}\frac{a}{W}Y^2\left(\frac{a}{W}\right)d\frac{a}{W} \tag{3-10}$$

From this equation we see that there are 2 different contributions to compliance: the integration constant C_0, which represents the specimen compliance without the notch, and the second term, which expresses the contribution to compliance due to the presence of the notch. The fact that we can separate these two contributions is the main assumption of this method. Proceeding with the derivation, we can obtain C_0 from the beam theory, and rewrite it as:

$$C_0 = \frac{\delta_{bending}}{P} + \frac{\delta_{shear}}{P} = \frac{15}{81}\frac{1}{E}\frac{L^3}{BW^3} + \frac{3}{8}\frac{1}{E}\frac{L}{BW}(2+\nu) \tag{3-11}$$

where ν is the Poisson's ratio. Finally, after some rearrangements, we get:

$$C\left(\frac{a}{W},t\right) = D(t)\frac{L}{BW}\left[\frac{15}{81}\left(\frac{L}{W}\right)^2 + \frac{3}{8}(2+\nu) + \frac{2\pi L}{W}\int_o^{\frac{a}{W}}\frac{a}{W}Y^2d\left(\frac{a}{W}\right)\right] \tag{3-12}$$

where $D(t)$ is the creep compliance of the material and has been added in place of the inverse of Young's modulus since we are dealing with viscoelastic materials. Among all these terms, there are only two of them which vary during a test, namely $D(t)$ and $\frac{a}{W}$. Based on that, we can rewrite Equation (3-12) as:

$$C\left(\frac{a}{W},t\right) = D(t)\phi\left(\frac{a}{W}\right) \tag{3-13}$$

where $\phi\left(\frac{a}{W}\right)$ is a geometry calibration factor. Also, before crack initiation, $\frac{a}{W}$ is not varying since the crack has constant length a_0. So, in that phase, the only varying quantity is the creep compliance. This is true for both sharp-notched specimens before crack initiation and for blunt-notched specimens for the whole duration of the test.

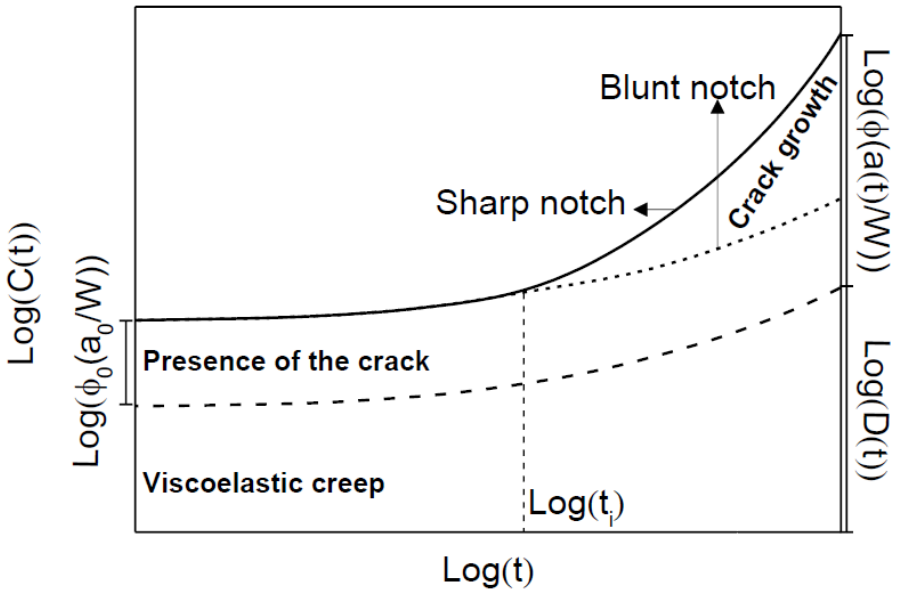

Figure 23: compliance vs. time during a test considering the presence of the notch depending on its nature [42]

This is shown in Figure 25.

Considering this, we can write for a blunt-notched specimen:

$$C_b\left(\frac{a_0}{W}, t\right) = D(t)\phi_0\left(\frac{a_0}{W}\right) \tag{3-14}$$

where C_b is the compliance of the blunt specimen and ϕ_0 is the geometry calibration factor computed before crack initiation (it is constant in time up to initiation) Dividing equation (3-13) by equation (3-14) we get:

$$\frac{C}{C_b} = \frac{\phi}{\phi_0} \tag{3-15}$$

Considering a blunt notched and a sharp notched specimen of the same dimensions, ϕ is equal to ϕ_0 up to crack initiation. The blunt specimen is built with the same dimension of the sharp one since by doing so any possible non-linearity should be

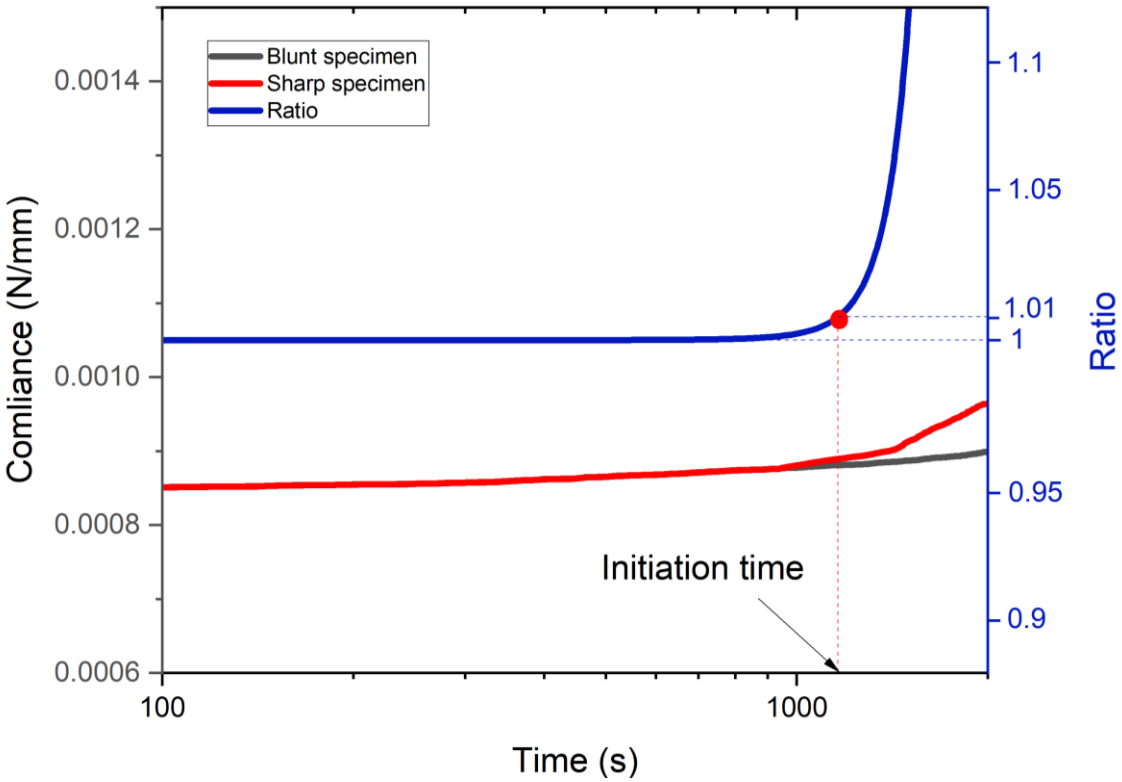

included in the evaluation of the compliance D(t). After crack initiation, however, the ratio between these 2 parameters starts increasing above unity because of crack propagation. By this consideration, we can detect crack initiation imposing a threshold on the $\frac{C}{C_b}$ ratio value. Here, a value of 1.01 has been selected. This is depicted in Figure 26.

Figure 24: Creep compliances of the blunt notched and sharp notched specimens, and ratio between them as a criterion to individuate initiation

Following this path, it is also possible to calculate the length of the crack during the test. We can do it by combining equation (3-15) and (3-12):

$$\phi_0 \frac{C}{C_b} = \phi = \frac{L}{BW}\left[\frac{15}{81}\left(\frac{L}{W}\right)^2 + \frac{3}{8}(2+\nu) + \frac{2\pi L}{W}\int_o^{\frac{a}{W}} \frac{a}{W} Y^2 d\left(\frac{a}{W}\right)\right] \qquad (3\text{-}16)$$

However, a small variation has been applied to this method. From the compliance of the blunt-notched specimen:

$$C_b\left(\frac{a}{W},t\right) = D(t)\phi_{0,b}\left(\frac{a}{W}\right) \tag{3-17}$$

the material compliance D(t) has been extrapolated, since $\phi_{0,b}\left(\frac{a}{W}\right)$ is constant during the test and can be easily computed knowing the specimen geometry. Multiplying it with $\phi_{0,s}\left(\frac{a}{W}\right)$, a compliance can be obtained, and it is the one corresponding to an hypothetical blunt specimen, on which fracture does not initiate, and has the dimensions of the sharp specimen under investigation. This will be referred to as dummy-blunt specimen:

$$C_{db}\left(\frac{a}{W},t\right) = D(t)\phi_{0,s}\left(\frac{a}{W}\right) \tag{3-18}$$

This was done in order to minimize the error that can arise from the fact that the specimen, although having the same nominal dimensions, are actually slightly different due to fabrication errors. So, finally, we have the equation:

$$\phi_{0,s}\frac{C}{C_{db}} = \phi = \frac{L}{BW}\left[\frac{15}{81}\left(\frac{L}{W}\right)^2 + \frac{3}{8}(2+\nu) + \frac{2\pi L}{W}\int_o^{\frac{a}{W}}\frac{a}{W}Y^2 d\left(\frac{a}{W}\right)\right] \tag{3-19}$$

This equation has been developed in Annex 1 and numerically solved for a using a purposedly made MATLAB script. These values of a were then used to compute the instantaneous crack speed at each time. Since the actual instantaneous speed-fracture parameter combination during a single experiment was not interesting because of their high dispersion caused by the noisiness of the data, an average value was computed for both the crack speed and the fracture parameter value for each tested specimen, and they will be reported in graphs by this value with associated error bars.

3.2 Constant displacement rate tests

The aim was again to obtain for each material K vs. t_i and K vs. $\dot{a}$ curves, in a different timeframe with respect to creep tests.

3.2.1 Initiation time and crack speed evaluation

In these type of tests, direct observation of the crack during the test was possible. Thanks to this, both the initiation and propagation phase can be characterized from recordings of the tests. To identify crack initiation and measure the crack length, an image processing MATLAB script has been developed, able to automatically identify the position of the crack tip during the experiments. An example of the process is reported in Figure 27.

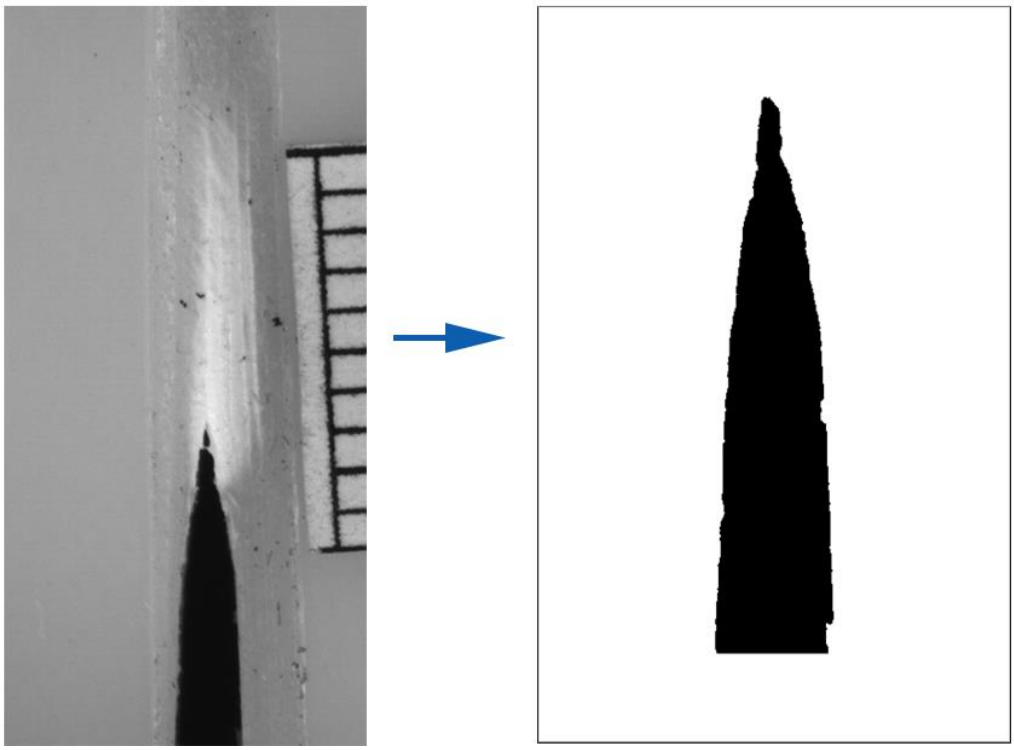

Figure 25: Image elaboration process applied to the recording of the experiments

Thanks to this, it was possible to measure the crack length frame-per-frame, and so also to identify the moment in which it starts propagating. It must be noted that often it was not possible to automate this process because of some artifacts in the image, for example the presence of some debris at the tip of the crack residual from the notching operation, so the analysis was always supported by a visual inspection of the recordings to validate the output of the script. After identifying the initiation time, the load acting on the specimen at that time was extracted from the output of the dynamometer and the corresponding value of the stress intensity factor and energy release rate at initiation was computed. For tests in active environment, even if the tank was equipped with a window, the presence of the oil made the use of this script impossible because of the blurring effect it caused. So, the initiation time and crack

speed for these tests has been determined by visually measuring the length of the crack from the frames of the recordings.

3.2.2 Stress intensity factor

The formula for the determination of the stress intensity factor was the same as the one used for creep tests, with the difference that the applied load is also here a function of time:

$$K = Y\left(\frac{a}{W}\right)\frac{P(t)L\sqrt{\pi a}}{B^{*}W^{2}} \tag{3-20}$$

3.2.3 Energy release rate

The formula was again the one used for the creep tests, with the difference that, being the load P not constant in time, U must be computed as an integral on the load-displacement curve:

$$U_t = \int_0^{\delta_t} P(\delta)d\delta \tag{3-21}$$

where U_t is the energy computed at time t. So, G can be computed at each desired instant as:

$$G = \frac{U_t}{BW}\cdot\frac{1}{\psi_{FPB}\left(\frac{a}{W}\right)} \tag{3-22}$$

4 MATLAB Scripts description

In this chapter, the two scripts written for this work are reported and commented. First the one for elaborating data from creep experiments, and then the one for constant displacement rate tests.

4.1 Creep data

4.1.1 Data loading

The script will automatically load the raw data. The requirements are to create in the same root folder of MATLAB:

- A folder named “Raw”, containing all raw data just as extracted from the creep machines.
- A folder named “Proc”, where the script once ran will save the processed propagation data
- An *xlsx* file named “Creepdata” containing a row for each analyzed specimen where there must be reported:
    - The specimen name. With the nomenclature chosen in this work names are composed by ESCR* or GP* if the specimen is made of HIPS 1 or HIPS 2 respectively. Then the letter “L” followed by a number which symbolizes the number of molded plate from which it has been machined, and finally a letter “S” if the specimen is a sharp notched one or “B” if a blunt notched one, with one final number symbolizing the the number of that specimen made from that plate.
    - B^* of the specimen
    - W of the specimen
    - a of the specimen
    - The zero value for the displacement recorded on the creep machine
    - The load (in Kg) applied to the specimen
    - The initiation time
    - The temperature of the test
    - The presence of the active environment, indicated by an “X” if it is present.

```
clear all
close all
clc

name_s= "GPL5S1";
```

This field must be modified inserting the name of the sharp notched specimen to analyze

```
SconstS=400;
SconstB=1000;
```

These fields are the moving-average smoothing constants that will be applied to the graphs of displacement vs. time.

```
T = readtable('Crepdata.xlsx');
map_id = find(T{:,1}==name_s);
```

The file containing specimen data gets loaded and the row index containing the chosen specimen is found.

```
zeroSharp=cell2mat(T.Zero(map_id));
zeroSharp=str2double(zeroSharp);

pesoSharp=cell2mat(T.Load(map_id));
pesoSharp=str2double(pesoSharp);

Bs = cell2mat(T.B_(map_id));
Bs = str2double(Bs);

a_0s = cell2mat(T.a(map_id));
a_0s = str2double(a_0s);

Ws = cell2mat(T.W(map_id));
Ws = str2double(Ws);

temp = T.T(map_id);

ti = T.ti(map_id);
```

All the data corresponding to the chosen specimen is loaded as a string and converted to double where necessary

```
type = char(name_s);
s = what('Tutto');
dirdir = s.path;
lab = type + " " + string(temp);
master_dir = dirdir;
if (type(1)=='G')
    %fprintf("G \n");
    if (temp == 31)
        fprintf("Loading %s \n",lab);
        fulladr_b = master_dir+"\GP L1 B2.txt"; %GP31°
        bfile="GPL1B2.txt";%GP31°
    else
        if (temp == 50)
            fprintf("Loading %s \n",lab);
            fulladr_b = master_dir+"\GPL3B2.txt"; %GP50°
            bfile="GPL3B2.txt";%GP50°
        else
            fprintf("Loading %s \n",lab);
            fulladr_b = master_dir+"\GPL3B1.txt"; %GP40deg
            bfile="GPL3B1.txt";%GP40deg
        end
```

```
    end
else
    %fprintf("E \n");
        if (temp == 31)
            fprintf("Loading %s \n",lab);
            fulladr_b = master_dir+"\ESCRL1B9.txt"; %ESCR31°
            bfile="ESCRL1B9.txt";%ESCR31°
        else
            if (temp == 50)
                fprintf("Loading %s \n",lab);
                fulladr_b = master_dir+"\ESCRL1B6.txt"; %ESCR50deg
                bfile="ESCRL1B6.txt";%ESCR50deg
            else
                fprintf("Loading %s \n",lab);
                fulladr_b = master_dir+"\ESCRL8B1.txt";%ESCR40°
                bfile="ESCRL8B1.txt";%ESCR40°
            end
        end
end

% Carica parametri Blunt (trova corrispondenza nome nel xlsx)
q = erase(bfile,".txt");
map_id_b = find(T{:,1}==q);

zeroBlunt=cell2mat(T.Zero(map_id_b));
zeroBlunt=str2double(zeroBlunt);

pesoBlunt=cell2mat(T.Load(map_id_b));
pesoBlunt=str2double(pesoBlunt);

B = cell2mat(T.B_(map_id_b));
B = str2double(B);

W = cell2mat(T.W(map_id_b));
W = str2double(W);

a_0 = cell2mat(T.a(map_id_b));
a_0 = str2double(a_0);
```

Here, the blunt specimen which has been tested in the same temperature and environment conditions as the chosen sharp one is identified and all its data together with its address in the folder is loaded.

```
di = dir([char(master_dir), '\*.txt']);
n=length(di());

for k =1 : n
file1 = getfield(di,{k},'name');
file_fetch = file1;
file1 = file1(1:end-4);
file1 = strrep(file1,'_','');
file1 = strrep(file1,'olio','');
file1 = strrep(file1,' ','');
file(k) = string(file1);
```

```
end

id_sh = find(file == name_s);
file_s = getfield(di,{id_sh},'name');
fulladr_s = convertCharsToStrings(master_dir) + "\"+file_s;
fprintf("Sharp: %s \n", file_s);
fprintf("Blunt: %s \n", bfile);

T_s = readmatrix(fulladr_s);
T_b = readmatrix(fulladr_b);
```

Finally, the address for the sharp notched specimen is found and both the sharp and blunt raw data are loaded as matrices of doubles.

Then, the second segment corresponding to the elaboration of the raw data begins.

4.1.2 Data elaboration

```
L = 55;
 nu = 0.41;
 a_0 = 14.95;
 Ls = 55;
 nus = 0.41;
c1=(15/81)*(Ls^2/Ws^2)+((3/8)*(2+nu));
c2=0.6272/Ws^2;
c3=-1.0379/Ws^3;
c4=4.5822/Ws^4;
c5=-9.9387/Ws^5;
c6=20.2267/Ws^6;
c7=-32.9577/Ws^7;
c8=47.0713/Ws^8;
c9=-40.7556/Ws^9;
c10=19.6/Ws^10;
```

This portion starts with some constants which will be used later to compute other parameters.

```
T_s(1,:) = [];
T_s(1,:) = [];
T_s(1,:) = [];
T_s(1,:) = [];
T_s(1,:) = [];
T_s(1,:) = [];
T_s(1,:) = [];
T_s(1,:) = [];
T_s(1,:) = [];
T_s(1,:) = [];
T_s(1,:) = [];
tempoRawS=T_s(:,1);
deformazioneRawS=T_s(:,2);
```

```
for j=1:length(deformazioneRawS)
deformazioneS(j)=deformazioneRawS(j)-zeroSharp;
end
deformazioneS=deformazioneS';
fs=0;
is=1;
while fs==0
 if deformazioneS(is)>0
     fs=1;
 end
 is=is+1;
end
for j=1:length(tempoRawS)
    tempoS(j)=tempoRawS(j)-tempoRawS(is-1);
end
tempoS=tempoS';
 deformazioneS=deformazioneS(is-1:length(deformazioneS),:);
 tempoS=tempoS(is-1:length(tempoS),:);
for j=1:length(deformazioneS)
    complianceS(j)=deformazioneS(j)/(pesoSharp*9.81);
end
complianceS=complianceS';
complianceS(isnan(complianceS))=0;
```

In this segment the compliance of the sharp-notched specimen is extracted as an array. First, the first 12 rows of the data coming from the raw file is discarded, since it does not contain useful information for the analysis. Then, 2 arrays are extracted containing the values of time and deformation extracted by the creep machines.

After this, from all the values in the deformation array, the zero value of the deformation is subtracted to obtain the effective displacement measured on the specimen. This array is analyzed to find the first value which is greater than 0, meaning that the weight has been effectively applied to the specimen. The index of the array corresponding to this condition is saved and it is used to impose that, in the array containing time values, the 0 value is corresponding to the start of the test. Finally, the 2 arrays are cut to keep only values corresponding to a time grater than 0, the only data which is meaningful for further elaborations. Finally, the compliance is computed by dividing the deformation by the force applied to it.

```
 T_b(1,:) = [];
 T_b(1,:) = [];
 T_b(1,:) = [];
 T_b(1,:) = [];
 T_b(1,:) = [];
 T_b(1,:) = [];
 T_b(1,:) = [];
 T_b(1,:) = [];
 T_b(1,:) = [];
 T_b(1,:) = [];
 T_b(1,:) = [];
```

```
 T_b(1,:) = [];
tempoRawB=T_b(:,1);
deformazioneRawB=T_b(:,2);
for j=1:length(deformazioneRawB)
deformazioneB(j)=deformazioneRawB(j)-zeroBlunt;
end
deformazioneB=deformazioneB';
fb=0;
ib=1;
while fb==0
 if deformazioneB(ib)>0
     fb=1;
 end
 ib=ib+1;
end
for j=1:length(tempoRawB)
    tempoB(j)=tempoRawB(j)-tempoRawB(ib-1);
end
tempoB=tempoB';
 deformazioneB=deformazioneB(ib-1:length(deformazioneB),:);
 tempoB=tempoB(ib-1:length(tempoB),:);
for j=1:length(deformazioneB)
    complianceB(j)=deformazioneB(j)/(pesoBlunt*9.81);
end
complianceB=complianceB';
%% Smoothing compliance
smoothS=movmean(complianceS,SconstS);
smoothB=movmean(complianceB,SconstB);
```

This portion is equal to the previous one but is applied to the blunt- notched specimen. In the end, both the compliances are smoothed used the smoothing constants previously defined.

```
semilogx(tempoB,smoothB)
hold on
semilogx(tempoS,smoothSout);
grid on
```

The compliances are then plotted. This is used to find the initiation time by visually looking for the time at which the compliance of the sharp-notched specimen starts deriving from blunt-notched one as described in the previous chapter. This method for the determination of the initiation time was chosen instead of an automatic one because the latter turned out to not be effective, given the noisiness of the data and the uncertainty in the determination of the zero value of displacement.

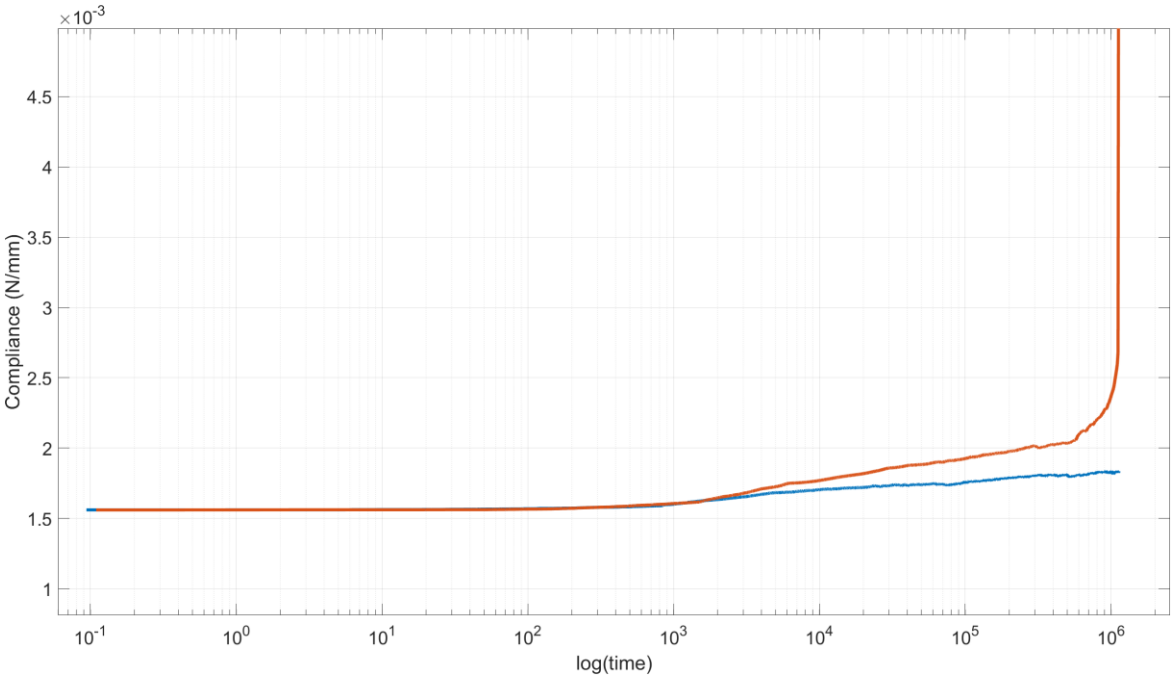

Figure 26: Compliance vs. time curve for blunt (in blue) and sharp (in orange) as output of the script

So, when analyzing a specimen for the first time, the script must be first run up to this point to determine the initiation time. This must then be inserted in the "*creepdata.xlsx*" file, and the script can then be run again to progress with the analysis.

```
tempoS(isnan(tempoS))=0;
smoothSout(isnan(smoothSout))=0;

tempoB(isnan(tempoB))=0;
vq=interp1(tempoS,smoothSout,tempoB);
vq(isnan(vq))=0;
vq(1)=vq(2);

innesco1=find(tempoB>ti-0.1);
innesco=innesco1(1);
verticalShift=vq(innesco)-smoothB(innesco);
smoothS2= vq-verticalShift;


funz=@(x) (a_0/W)*(1.12-(1.39.*a_0./W)+(7.32.*(a_0/W).^2)-
(13.1.*(a_0/W).^3)+(14.*(a_0/W).^4))^2;
xmin=0;
xmax=a_0/W;
integ=integral(funz,xmin,xmax,'ArrayValued',true);
fizero=(L/(B*W))*((15/81)*(L^2/W^2)+((3/8)*(2+nu))+(2*pi*L/W)*integ);
%calcolo phi zero per blunt

funzs=@(y) (a_0s/W)*(1.12-(1.39.*a_0s./Ws)+(7.32.*(a_0s/Ws).^2)-
(13.1.*(a_0s/Ws).^3)+(14.*(a_0s/Ws).^4))^2;
xmins=0;
xmaxs=a_0s/Ws;
```

```
integ=integral(funzs,xmins,xmaxs,'ArrayValued',true);
fizeros=(Ls/(Bs*Ws)).*(c1+(2*pi*Ls/Ws).*(c2.*a_0s.^2 +c3.*a_0s.^3
+c4.*a_0s.^4 +c5.*a_0s.^5 +c6.*a_0s.^6 +c7.*a_0s.^7 +c8.*a_0s.^8
+c9.*a_0s.^9 +c10.*a_0s.^10));


for j=1:length(smoothS2)
   rapporto(j)=smoothS2(j)/smoothB(j);
   fi(j)=rapporto(j)*fizeros;
end
fi=fi';
for j=1:length(fi)
    d(j)=smoothB(j)/fizeros;
end
d=d';
for j=1:length(d)
    sharpfittizio(j)=d(j)*fizeros;
end
sharpfittizio=sharpfittizio';
for j=1:length(smoothS2)
    phi(j)=(smoothS2(j)/sharpfittizio(j))*fizeros;
end
phi=phi';
```

In this segment the aim is to extract the function ϕ as expressed in (3-19). The steps taken are the ones described in Chapter 3, passing through the definition of a dummy specimen.

```
a = zeros(length(phi),1);
syms fun(a);
fun(a)=  (Ls/(Bs*Ws)).*(c1+(2*pi*Ls/Ws).*(c2.*a.^2 +c3.*a.^3 +c4.*a.^4
+c5.*a.^5 +c6.*a.^6 +c7.*a.^7 +c8.*a.^8 +c9.*a.^9 +c10.*a.^10));

k=1;
while k < length(phi)-innesco
    fun=@(a) (Ls/(Bs*Ws)).*(c1+(2*pi*Ls/Ws).*(c2.*a.^2 +c3.*a.^3 +c4.*a.^4
+c5.*a.^5 +c6.*a.^6 +c7.*a.^7 +c8.*a.^8 +c9.*a.^9 +c10.*a.^10))-
phi(k+innesco-1);
    S(k)=fzero(fun,15);
    tempoA(k)=tempoB(k)-tempoB(innesco);
    if S(k)>Ws*0.6
    k=length(phi);
    end
     k=k+1;
end
tempoA=tempoA';
shift=a_0s-S(1);
for j=1:length(S)
   S(j)=S(j)+shift;
end
S=S';
h=0;
j=1;
```

```
while h==0
    if    S(j)< Ws*0.6 && j<length(S)-1
       crack(j)=S(j);
       tempoCrack(j)=tempoA(j);
       j=j+1;
    else
        h=1;
    end

end
crack = crack';
tempoCrack=tempoCrack';
avanzamento=[tempoCrack,crack];
smoothC=movmean(crack,20);

diff=diff';
[x_fit, gof] =createFit(tempoCrack,smoothC);
k=1;
for j=tempoCrack(1):(tempoCrack(length(tempoCrack))-
tempoCrack(1))/100:tempoCrack(length(tempoCrack))
   crackT(k)=j;
   clength(k)=x_fit(crackT(k));
   k=k+1;
end
clength=clength';
cdiff=clength(1)-a_0s;
for j=1:length(clength)
   clength(j)=clength(j)-cdiff;
end
clength=clength';
crackT=crackT';
for j=1:length(clength)-1
    diffc(j)=(clength(j+1)-clength(j))/(crackT(j+1)-crackT(j));
    diffc(j+1)=diffc(j);
end
for k=1:length(clength)
    y(k)=1.12-(1.39*clength(k)/Ws)+(7.32*(clength(k)/Ws)^2)-
(13.1*(clength(k)/Ws)^3)+(14*(clength(k)/Ws)^4);
   kout(k)= (y(k)*Ls*pesoSharp*9.81*sqrt(pi*clength(k)/1000))/(Bs*Ws^2);
end
formaG =@(x) (Ws*((3*(2 + nus))/8 + (5*Ls^2)/(27*Ws^2)
+(2*Ls*3.14/Ws)*(0.6272*x^2-1.03787*x^3+4.58223*x^4-
9.93872*x^5+20.2267*x^6-32.9577*x^7+47.0713*x^8-
40.7556*x^9+19.6*x^10)))/(2*Ls*3.14*(1.2544*x-3.1136*x^2+18.3289*x^3-
49.6936*x^4+121.36*x^5-230.704*x^6+376.57*x^7-366.8*x^8+196*x^9));

for k=1:length(clength)
   yG(k)= formaG(clength(k)/Ws);
   G(k)=1000*U/(Bs*Ws*yG(k));
end
kout=kout';
```

In this final segment, the ϕ function is numerically solved to obtain the value of the crack length at any instant following the crack initiation up until the point at which

the condition is satisfied where this analysis would not be valid. Then, an exponential fit has been applied to these data in order to improve data quality removing noise, and using these values combined with the corresponding values of time, the differential has been computed to obtain the value of crack speed at any instant. Finally, the values of crack length obtained are used to compute at any point K and G, passing through their relative shape factors.

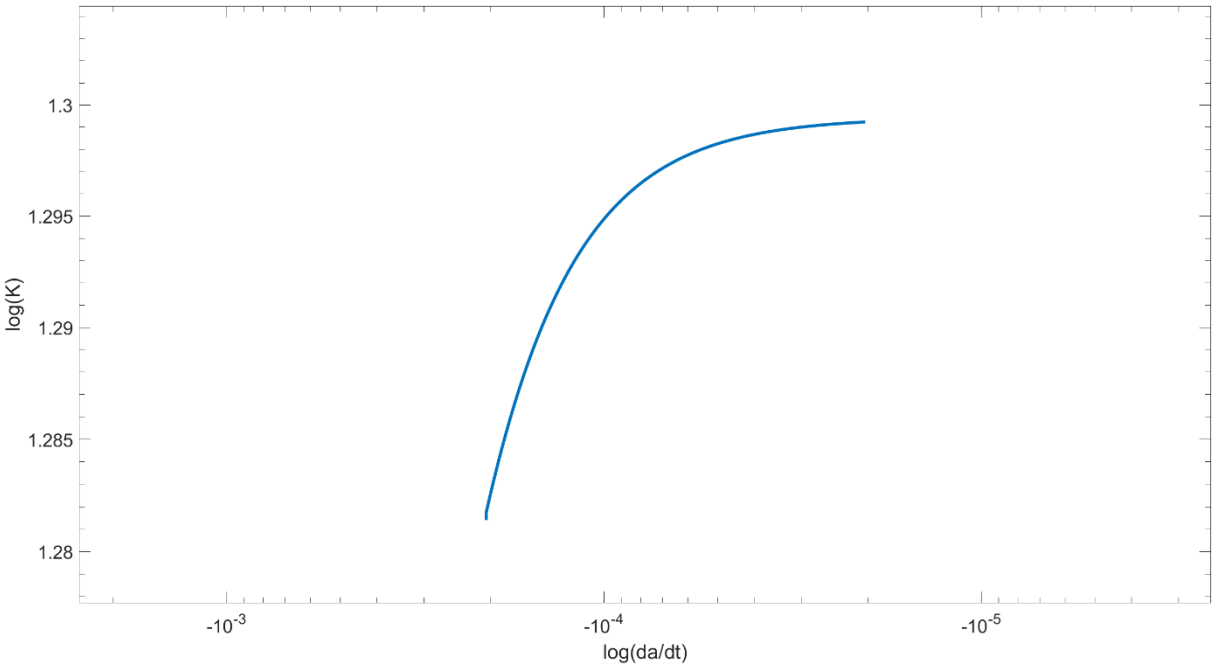

Figure 27: output of the script as K vs. crack speed

4.1.3 Output creation

```
NE=find(diffc<=0);
diffc(NE)=[];
kout(NE)=[];
G(NE)=[];
prova = char(name_s);
s = what('Proc');
adr = s.path;
matA = [log10(diffc)', log10(kout)];
matB = [log10(diffc)', log10(G)'];

fname1 = name_s + "_" + temp+"diffC_K.csv";
fname2 = name_s + "_" + temp+"diffC_G.csv";

lab1 = adr + "\" +fname1;
lab2 = adr + "\" +fname2;
```

```
csvwrite(lab1,matA);
csvwrite(lab2,matB);

fprintf("%s saved \n",fname1);
fprintf("%s saved \n",fname2);

figure();
loglog(diffc,kout);
figure();
loglog(diffc,G);
```

In this final portion of the script the output files are created. For each specimen 2 .csv files are created: one containing the value of crack speed combined with the instantaneous value of K, and the other one with the corresponding value of G.

4.2 Constant displacement rate tests

```
clear all
clc
close all
threshold=30;
scale=91.842;
Ls=55;
Ws=29.67;
Bs=3.23;
a0=15.07;
ti=0;
FPS=20;
pesoSharp=310;
```

The code starts with some constants that will have to be adjusted for each specimen, in particular:

- Threshold: it is the threshold used to distinguish a pixel from white to black, it should be in the range 20-40 depending on the brightness of the video
- Scale: is the scale of the image expressed as pixel/mm
- Ls: is the distance between the two upper pins, in all experiments has been fixed at 55mm.
- Ws, Bs, a0, ti: the geometric dimensions of the specimen and the initiation time, which should be determined by watching the recording of the experiment.
- FPS: the frames per second of the recording, they vary depending on the expected duration of the experiment
- pesoSharp: the load in Newton applied to the specimen at the initiation time. This can be a rough value determined by looking at the curve, the precise value will be extracted later starting from this.

```
bfile="C:\Users\....csv";
b=readmatrix(bfile);
Loadsraw=b(:,3);
innescoloadm=find(Loadsraw>=pesoSharp);
innescoload=innescoloadm(1);
Loadsraw(1:innescoload,:)=[];
```

Here the .csv file of the raw load vs. time is open and values are loaded. Then, the precise value of the initiation load is extracted as the value subsequent to the rough one inserted in the beginning.

```
master_dir = uigetdir([]);
d = dir([char(master_dir), '\*.jpg']);
imds = imageDatastore(master_dir, 'FileExtensions','.jpg');
```

In this segment the video is loaded in the script. To do so, it is necessary to convert the recording to a series of .jpg images, and when the script is launched, a prompt asking to select a folder will open. The folder where the images are saved must be selected.

```
for ii = 1:length(imds.Files)
    Ia(:,:,ii) = imcrop(rgb2gray(readimage(imds,ii)),[229 900 246 1281]);
    Q = Ia(:,:,ii);
    Q(Q<=threshold)=0;
    Q(Q>threshold)=65555;
    Ia(:,:,ii)=Q;
    Id(:,:,ii) = im2double(Ia(:,:,ii));
    fprintf('Loading image: %i \n',ii);
    c=false;
i=1;
while c==false
    for j=1:length(Ia(1,:,ii))
        if Ia(i,j,ii)==0
            c=true;
        end;
    end;
        top(ii)=i;
        i=i+1;
end;
```

Here each image is loaded, is transformed to a grey scale image and is cropped. The crop zone must be defined manually by modifying the coordinates in square brackets is the second line. This must be done making sure to exclude from the selection anything but the crack itself and the white portions of the specimen to avoid artifacts. The cropped image is then edited in order to transform the scale of grey in just a black and white image, distinguishing black and white based on the threshold previously chosen. In the 2 following cycles, the image is checked pixel-by-pixel individuating the coordinate of the first black pixel (the tip of the crack). Doing this, an array is created containing the position of the tip of the crack at any frame in the video.

```
end
for j=ti+1:length(top)
    tip(j-ti)=-top(j);
end
x=1:1:length(top);
zero=tip(1);
for j=1:length(tip)
   tip(j)=((tip(j)-zero)/scale)+a0;

   time(j)=x(j)/FPS;
end
```

In this portion the array previously obtained is modified in order for the crack length to be expressed in millimeters and to be starting from 0. An array of the time is also created by simply defining an incremental array and resizing it using the FPS value.

```
fine=find(tip>Ws*0.6);
tip(:,fine:length(tip))=[];
time(:,fine:length(time))=[];
cracktip=movmean(tip,5);
```

```
[x_fit, gof]=createFit(time,cracktip);
crack=x_fit(time);
```

Here the array of the crack length and time are cut when the usual condition of $\frac{a}{W} \geq 0.6$ is met, and a fit is created to smooth the obtained curve for further elaboration.

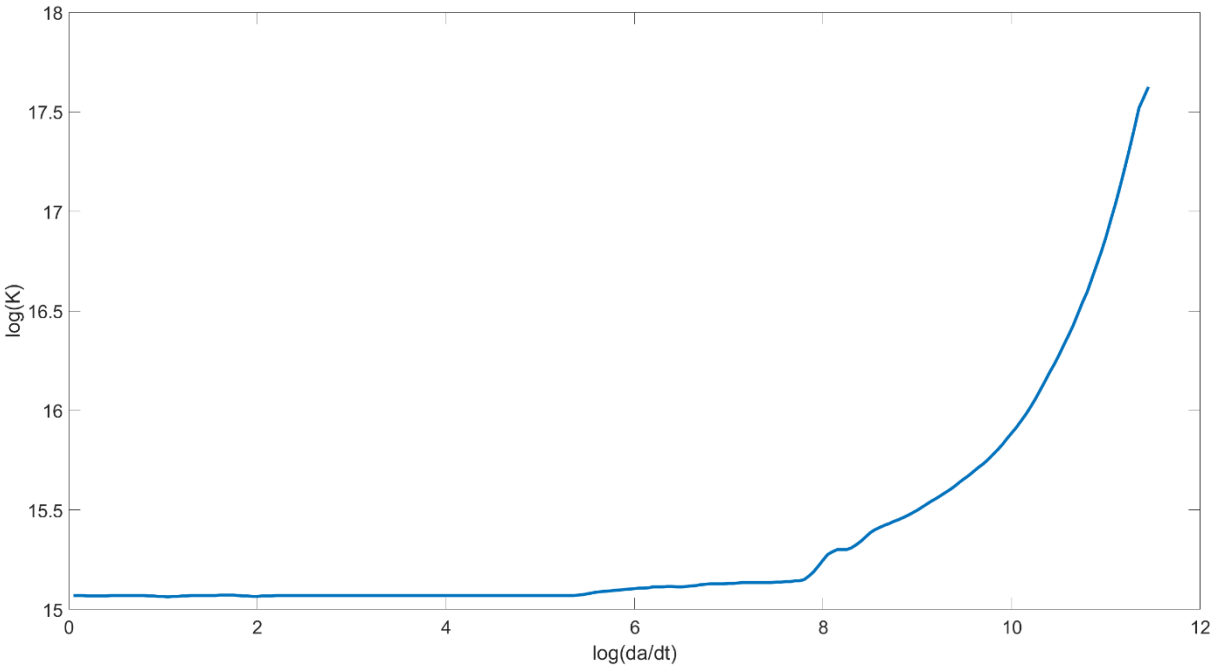

Figure 28: crack length vs. time as output of the script

```
for j=1:length(time)-1
    diffc(j)=(crack(j+1)-crack(j))/(time(j+1)-time(j));
    diffc(j+1)=diffc(j);
end
for k=1:length(time)
    y(k)=1.12-(1.39*crack(k)/Ws)+(7.32*(crack(k)/Ws)^2)-
(13.1*(crack(k)/Ws)^3)+(14*(crack(k)/Ws)^4);
   kout(k)= (y(k)*Ls*Loadsraw(k)*sqrt(pi*crack(k)/1000))/(Bs*Ws^2);
end
```

Finally, the differential for each point is computed to determine the instantaneous crack speed, and the corresponding value of K.

5 Conclusions

The fracture behavior and environmental stress cracking resistance at different temperatures of two different HIPS grades, a general purpose one and an ESC-resistant one, were evaluated using a LEFM approach. Fracture was analyzed considering both the initiation phase (through the initiation time) and the propagation one (through the crack speed), using as a fracture parameter both K and G. Test were conducted at 23, 31, 40 and 50°C . Tests were conducted in 2 different configurations: constant load and constant displacement rate.

For each configuration, an attempt has been made to create a MATLAB script able to automate the analysis of the crack initiation and propagation phase starting directly from raw data.

The results obtained with these scripts are found to be comparable with the ones obtained by elaborating the data for each test manually, in the average. However, some of the obtained raw data has more noise than other or presents some artifacts coming from a malfunction of the machines, and to identify these cases and make sure these occurrences do not interfere with the goodness of the elaboration, going over them manually is the best choice.

It must be noted that using the script for creep tests, the smoothing constant plays an important role in finding the initiation time. A certain level of smoothing is needed in order to get rid of the noise, but excessive smoothing can lead to an alteration of the obtained curve.

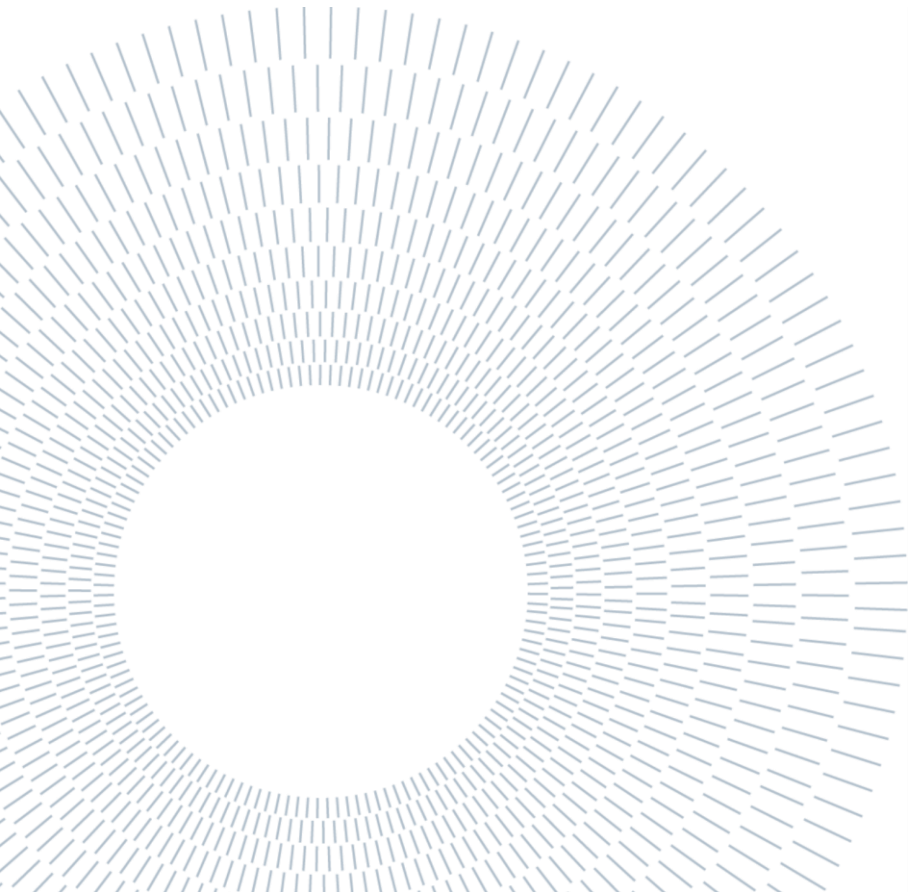

Bibliography

[1] R. B. Seymour, «Origin and Early Development of Rubber-Toughened Plastics,» pp. 3-13, 1989.

[2] X. Wang, K. Zhao e H. Zhao, «Finite element simulation of biofilm viscoelastic behavior under various loadings,» *Journal of Mechanics in Medicine and Biology*, vol. 18, n. 5, p. 1850056, 2018.

[3] A. V. Tobolsky, «Stress relaxation studies of the viscoelastic properties of polymers,» *Journal of Applied Physics*, vol. 27, n. 2, pp. 673-685, 1956.

[4] P. B. Bowden e J. A. Jukes, «The plastic flow of isotropic polymers,» *Journal of Materials Science*, vol. 7, n. 1, pp. 52-63, 1972.

[5] E. J. Kramer, «Microscopic and molecular fundamentals of crazing,» *Crazing in polymers. Springer, Berlin, Heidelberg*, pp. 1-56, 1983.

[6] R. Frassine, «Mechanical behavior of polymers,» *course handouts.*

[7] R. Bagheri e R. Pearson, «Role of particle cavitation in rubber-toughened epoxies: 1. Microvoid toughening,» *Polymer 37.20*, pp. 4529-4538, 1996.

[8] A. S. Argon, «The physics of deformation and fracture of polymers,» *New York.: Cambridge*, 2013.

[9] L. Andena, L. Castellani, A. Castiglioni, A. Mendogni, M. Rink e F. Sacchetti, «Andena, Luca, et al. "Determination of environmental stress cracking resistance of polymers: Effects of loading history and testing configuration,» *Engineering Fracture Mechanics,* vol. 101, pp. 33-46, 2013.

[10] M. A. Kamaludin, «Characterising the environmental stress».

[11] L. M. Robeson, «Environmental Stress Cracking: A Review,» *Polymer Engineering & Science,* vol. 53, n. 3, pp. 453-467, 2013.

[12] «ASTM D 1693».

[13] R. O. Ritchie e D. Liu, «Introduction to fracture mechanics,» *Elsevier,* 2021.

[14] D. Y. Yevgeny e G. V. Lasko, «Field of Stresses in an Isotropic Plane with Circular Inclusion under Tensile Stress,» 2012.

[15] C. E. Inglis, «Stresses in a plate due to the presence of cracks and sharp corners,» *Trans Inst Naval Archit ,* vol. 55, pp. 219-241, 1913.

[16] A. A. Griffith, «VI. The phenomena of rupture and flow in solids,» *Philosophical transactions of the royal society of london. Series A, containing papers of a mathematical or physical character,* vol. 221, n. 582-593, pp. 163-198, 1921.

[17] G. R. Irwin, «Fracture Dynamics,» *Fracturing of metals,* 1947.

[18] G. R. Irwin, «Onset of fast crack propagation in high strength steel and aluminum alloys,» *Naval Research Lab Washington DC,* 1956.

[19] H. M. Westergaard, «Bearing pressures and cracks: Bearing pressures through a slightly waved surface or through a nearly flat part of a cylinder, and related problems of cracks,» pp. 49-53, 1939.

[20] G. R. Irwin, «Analysis of stresses and strains near the end of a crack traversing a plate,» pp. 361-364, 1957.

[21] M. L. Williams, «On the Stress Distribution at the Base of a Stationary Crack,» pp. 109-114, 1957.

[22] D. Kujawski e E. Fernand, «On the size of plastic zone ahead of crack tip,» *Engineering fracture mechanics,* vol. 25, n. 2, pp. 229-236, 1986.

[23] G. I. Barenblatt, «The mathematical theory of equilibrium cracks in brittle fracture,» *Advances in applied mechanics,* n. 7, pp. 55-129, 1962.

[24] F. M. Burdekin e S. D. E. W., «The crack opening displacement approach to fracture mechanics in yielding materials,» *Journal of Strain Analysis,* vol. 1, n. 2, pp. 145-153, 1966.

[25] J. R. Rice, «A path independent integral and the approximate analysis of strain concentration by notches and cracks,» pp. 379-386, 1968.

[26] C. F. Shih e W. Hutchinson, «Fully Plastic Solutions and Large Scale Yielding Estimates for Plane Stress Crack Problems,» pp. 289-295, 1976.

[27] G. R. Irwin e K. J. A., «Critical energy rate analysis of fracture strength,» *Spie Milestone series MS,* vol. 137, n. 136-141, p. 29, 1997.

[28] J. G. Williams e G. P. Marshall, «Environmental crack and craze growth phenomena in polymers,» *Proceedings of the Royal Society of London. A. Mathematical and Physical Sciences,* vol. 342, n. 1628, pp. 55-77, 1975.

[29] M. K. V. Chan e W. J. G., «Slow stable crack growth in high density polyethylenes,» *Polymer,* vol. 24, n. 2, pp. 234-244, 1983.

[30] K. Tonyali e B. Hugh R., «On the applicability of linear elastic fracture mechanics to environmental stress cracking of low-density polyethylene,» *Journal of materials science,* vol. 21, n. 9, pp. 3116-3124, 1986.

[31] M. Rink, R. Frassine, P. Mariani e G. Carianni, «Effects of detergent on crack initiation and propagation in polyethylenes,» *European Structural Integrity Society,* vol. 32, pp. 103-114, 2003.

[32] V. Altstaedt, S. Keiter, M. Renner e A. Schlarb, «Environmental stress cracking of polymers monitored by fatigue crack growth experiments.,» *Macromolecular Symposia,* vol. 214, n. 1, 2004.

[33] L. Andena, L. Castellani, A. Castiglioni, A. Mendogni, M. E. Rink Sugar, F. R. Sacchetti e A. Adib, «Environmental crack initiation and propagation in polyethylene under different loading conditions,» *15th International Conference on Deformation, Yield and Fracture of Polymers,* 2012.

[34] L. Andena, M. Rink, C. Marano, F. Briatico-Vangosa e L. Castellani, «Effect of processing on the environmental stress cracking resistance of high-impact polystyrene,» *Polymer Testing,* vol. 54, pp. 40-47, 2016.

[35] M. A. Kamaludin, Y. Patel, J. G. Williams e B. R. K. Blackman, «A fracture mechanics approach to characterising the environmental stress cracking behaviour of thermoplastics,» *Theoretical and Applied Fracture Mechanics* , vol. 92, pp. 373-380, 2017.

[36] M. A. Kamaludin, «Characterising the environmental stress cracking behaviour of thermoplastics: a fracture mechanics approach,» *Diss. Imperial College London,* 2017.

[37] M. Contino, L. Andena, V. La Valle, M. Rink, G. Marra e S. Resta, «A comparison between K and G approaches for a viscoelastic material: the case of environmental stress cracking of HDPE,» *Mechanics of Time-Dependent Materials,* vol. 24, n. 3, pp. 381-394, 2020.

[38] M. Contino, L. Andena, M. Rink, G. Marra e S. Resta, «Time-temperature equivalence in environmental stress cracking of high-density polyethylene,» *Engineering Fracture Mechanics,* vol. 203, pp. 32-43, 2018.

[39] V. G. Grassi, M. F. Dal Pizzol, M. M. C. Forte e S. C. Amico, «Influence of small rubber particles on the environmental stress cracking of high impact polystyrene,» *Journal of Applied Polymer Scienc,* vol. 121, n. 3, pp. 1697-1706, 2011.

[40] A. Mendogni, «Studio del comportamento a frattura in ambiente attivo di polistirene antiurto,» 2011.

[41] D. P. Rooke e C. David John, «Compendium of stress intensity factors,» *Procurement Executive, Ministry of Defence. H. M. S. O.,* p. 330, 1976.

[42] M. Contino, «Long term fracture behaviour of HDPE for household detergent containers: a study on environmental stress cracking,» *PhD dissertation.*

[43] «ISO22088-3: Plastics».

[44] T. L. Anderson, «Fracture Mechanics: Fundamentals and Applications,» *CRC Press,* 2017.

[45] G. M. Boyd, «Brittle fracture in steel structures,» *Elsevier,* 2016.

A. Calibration functions

A1: Geometry calibration function for the four-point bending configuration

The compliance of a notched specimen can be described as the product of the material creep compliance and of a geometry function written as:

$$\phi\left(\frac{a}{W}\right) = \frac{L}{BW}\left[\frac{15}{81}\left(\frac{L}{W}\right)^2 + \frac{3}{8}(2+\nu) + \frac{2\pi L}{W}\int_o^{\frac{a}{W}} \frac{a}{W} Y^2 d\left(\frac{a}{W}\right)\right] \qquad \text{(A-1)}$$

Where L is the span between the lower pins, B is the specimen thickness, W is the specimen width, ν is the material's Poisson's ratio and Y is the shape factor which is in this case equal to:

$$Y = 1.12 - 1.39\left(\frac{a}{W}\right) + 7.32\left(\frac{a}{W}\right)^2 - 13.1\left(\frac{a}{W}\right)^3 + 14.0\left(\frac{a}{W}\right)^4 \qquad \text{(A-2)}$$

which can then be squared and inserted in equation (A-1) giving:

$$\int_0^{\frac{\bar{a}}{W}} \frac{a}{W} Y^2\left(\frac{a}{W}\right) d\frac{a}{W} = \int_0^{\frac{\bar{a}}{W}} \left[1.2544\left(\frac{a}{W}\right) - 3.1136\left(\frac{a}{W}\right)^2 + 18.3289\left(\frac{a}{W}\right)^3 - 49.6936\left(\frac{a}{W}\right)^4 + 121.3604\left(\frac{a}{W}\right)^5 - 230.704\left(\frac{a}{W}\right)^6 + 376.57\left(\frac{a}{W}\right)^7 - 366.8\left(\frac{a}{W}\right)^8 + 196\left(\frac{a}{W}\right)^9\right] d\frac{a}{W} \qquad \text{(A-3)}$$

Solving this equation and inserting it in equation (A-1) the final expression for the calibration factor can be obtained:

$$\phi\left(\frac{a}{W}\right)=\frac{L}{BW}\cdot\left\{\frac{15}{81}\cdot\frac{L^2}{W^2}+\frac{3}{8}\cdot(2+\nu)+\frac{2\pi L}{W}\cdot\left[0.6272\left(\frac{a}{W}\right)^2-\right.\right.$$
$$1.0379\left(\frac{a}{W}\right)^3+4.5822\left(\frac{a}{W}\right)^4-9.9387\left(\frac{a}{W}\right)^5+20.2267\left(\frac{a}{W}\right)^6- \quad \text{(A-4)}$$
$$\left.\left.32.5537\left(\frac{a}{W}\right)^7+47.0713\left(\frac{a}{W}\right)^8-40.7556\left(\frac{a}{W}\right)^9+19.6\left(\frac{a}{W}\right)^{10}\right]_0^{\frac{\bar{a}}{W}}\right\}-$$

A2: Energy calibration factor for the four point bending configuration

The energy calibration factor can be computed as:

$$\psi\left(\frac{a}{W}\right)=\frac{C}{\frac{dC}{d\left(\frac{a}{W}\right)}} \quad \text{(A-5)}$$

where C is expressed as:

$$C=D(t)\cdot\phi\left(\frac{a}{W}\right) \quad \text{(A-6)}$$

With D being the material creep compliance and $\phi\left(\frac{a}{W}\right)$ the geometry calibration factor computed as equation (A-4). The derivative of the compliance can be evaluated as:

$$\frac{C}{\frac{dC}{d\left(\frac{a}{W}\right)}}=D\cdot\frac{d(\phi)}{d\left(\frac{a}{W}\right)}=D\frac{L}{BW}\cdot\left\{\frac{2\pi L}{W}\left[1.2544\left(\frac{a}{W}\right)-3.1136\left(\frac{a}{W}\right)^2+\right.\right.$$
$$18.3289\left(\frac{a}{W}\right)^3-49.6936\left(\frac{a}{W}\right)^4+121.3604\left(\frac{a}{W}\right)^5-230.704\left(\frac{a}{W}\right)^6+ \quad \text{(A-7)}$$
$$\left.\left.376.57\left(\frac{a}{W}\right)^7-366.8\left(\frac{a}{W}\right)^8+196\left(\frac{a}{W}\right)^9\right]\right\}$$

which introduced in equation (A-5) gives the final expression for the energy calibration factor:

$$\psi_{FPB}\left(\frac{a}{W}\right)=\left\{\frac{15}{81}\cdot\frac{L^2}{W^2}+\frac{3}{8}\cdot(2+\nu)+\frac{2\pi L}{W}\left[0.6272\left(\frac{a}{W}\right)^2-1.0379\left(\frac{a}{W}\right)^3+\right.\right.$$
$$4.5822\left(\frac{a}{W}\right)^4-9.9387\left(\frac{a}{W}\right)^5+20.2267\left(\frac{a}{W}\right)^6-32.9577\left(\frac{a}{W}\right)^7+ \quad \text{(A-8)}$$
$$\left.\left.47.0713\left(\frac{a}{W}\right)^8-40.7556\left(\frac{a}{W}\right)^9+19.6\left(\frac{a}{W}\right)^{10}\right]\right\}\cdot\left\{\frac{2\pi L}{W}\left[1.2544\left(\frac{a}{W}\right)-\right.\right.$$

$$3.1136\left(\frac{a}{W}\right)^2 + 18.3289\left(\frac{a}{W}\right)^3 - 49.6936\left(\frac{a}{W}\right)^4 + 121.3604\left(\frac{a}{W}\right)^5 - 230.704\left(\frac{a}{W}\right)^6 + 376.57\left(\frac{a}{W}\right)^7 - 366.8\left(\frac{a}{W}\right)^8 + 196\left(\frac{a}{W}\right)^9\Big]\Big\}^{-1}$$

List of Figures

List of Tables